CRONOSOJA: a daily time-step hierarchical model predicting soybean development across maturity groups in the Southern Cone

Alan D. Severini[1,*] Santiago Álvarez-Prado[2,3] María E. Otegui[4,3,1]
Monika Kavanová[5] Claudia R. C. Vega[6] Sebastián Zuil[7] Sergio Ceretta[5]
Martín Acreche[8,3] Fidencia Amarilla[9] Mariano Cicchino[10]
María E. Fernández-Long[4] Aníbal Crespo[4] Román Serrago[4,3] Daniel J. Miralles[4,3]

Abstract

Accurate prediction of phenology is the most critical aspect for the development of models aimed at estimating seed yield, particularly in species that exhibit variable sensitivity to environmental factors throughout the cycle and among genotypes. With this purpose, we evaluated the phenology of 34 soybean varieties in 43 field experiments located in Argentina, Uruguay, and Paraguay. Experiments covered a broad range of maturity groups (2.2-6.8), sowing dates (from spring to summer), and latitude range (24.9-35.6 °S), thus ensuring a wide range of thermo-photoperiodic conditions during the growing season. Based on the observed data, daily time-step models were developed and tested, first for each genotype, and then across maturity groups. We identified base temperatures specific for different developmental stages and an extra parameter for calculating the photoperiod effect after the R1 stage (flowering). Also, an optimum photoperiod length for each maturity group was found. Model selection showed that the determinants of phenology across maturity groups were mainly affecting the duration of vegetative and early reproductive stages. Even so, early phases of development were better predicted than later ones, particularly in locations with cool growing seasons, where the model tended to overestimate their duration. Overall, we developed a soybean phenology model that, owing to its process-based nature, is able to simulate phenology well across widespread locations and sowing dates yet, because of its simplicity, can be adopted by a wide audience. The final model was made available at http://cronosoja.agro.uba.ar.

[1] INTA. Centro Regional Buenos Aires Norte. Estación Experimental Agropecuaria Pergamino. Argentina
[2] Universidad Nacional de Rosario. Argentina
[3] Consejo Nacional de Investigaciones Científicas y Técnicas (CONICET), Argentina
[4] Facultad de Agronomía, Universidad de Buenos Aires. Argentina
[5] INIA La Estanzuela. Uruguay
[6] INTA. Centro Regional Córdoba. Estación Experimental Agropecuaria Manfredi. Argentina
[7] INTA. Centro Regional Santa Fe. Estación Experimental Agropecuaria Rafaela. Argentina
[8] INTA. Centro Regional Salta Jujuy. Estación Experimental Agropecuaria Salta. Argentina
[9] Centro de Investigación Capitán Miranda, Instituto Paraguayo de Tecnología Agraria, Itapúa, Paraguay
[10] INTA. Centro Regional Buenos Aires Sur. Estación Experimental Cuenca del Salado. Argentina

[*] Correspondence: Alan D. Severini <severini.alan@gmail.com>

1 Introduction

High efficiency in the use of resources to obtain the highest net margin per unit area, in an environmentally sustainable structure, is necessary in non-subsidised economies. This has led to farming systems relying on more intensive use of land and reduced tillage. In Argentina and Uruguay, double-cropping soybean after wheat or barley is a key component of these systems; but delaying soybean planting beyond the optimum date determine reductions in yield of soybean up to 50 kg ha^{-1} day^{-1} for high latitude environments (Calviño et al., 2003). Yield losses in soybean caused by delayed sowing date can be partially mitigated by changing the maturity group (MG) of the cultivar, thus changing

the sensitivity to photoperiod and consequently the length and timing of developmental stages. These changes allow adjusting soybean phenology to each specific environmental condition, which is crucial for avoiding yield losses.

Crop adaptation based on phenology is important for facing stressful environments. For instance, if flowering is too early, plant growth may be insufficient to produce a minimum level of biomass compatible with reasonable levels of yield (Mayers et al., 1991). Therefore, in those conditions where the growing season is extremely short (e.g. soybean at late sowing dates or at relatively high latitudes for a tropical crop) early vigour of the crop is far more important than the use of "full season" crops, which may delay flowering and reduce the period available for grain filling (Lawn et al., 1995). The mentioned extremes define the length of the growing season, and pre-flowering development may be manipulated to improve adaptation through balancing the optimum time of flowering and the consequent duration of pre- and post-flowering phases.

The main environmental factors identified as drivers of soybean development are photoperiod and temperature (Cober et al., 2001). Soybean is described as a "quantitative short day plant" as the maximum rate of development is observed when plants are exposed to short-day conditions (i.e. below a threshold or optimum photoperiod). The rate of development is reduced when the photoperiod is greater than the optimum value (Summerfield, 1998). Photoperiod sensitivity and optimum photoperiod values show variations with the maturity group. Cultivars from low maturity groups present a lower sensitivity and a higher optimum photoperiod than genotypes of high maturity groups (Summerfield, 1998). Temperature per se is the other factor affecting the rate of development which is the only one that has a universal impact on the rates of development (Aitken, 1974), meaning that all crops and all phases of development are sensitive to temperature (Miralles and Slafer, 1999). In general, the higher the temperature the faster the rate of development and consequently the shorter the time to complete a particular developmental phase (Garner and Allard, 1930; Miralles and Slafer, 1999; Slafer and Rawson, 1994).

In soybean, as in many other crops, the number of grains per unit area is the yield component best correlated with yield variations (Egli, 1998). Although the number of grains per unit area is determined throughout the crop cycle, this yield component in soybean is largely determined by the events occurring soon after flowering up to early seed filling (i.e. from R3 to R6 according to the scale of Fehr and Caviness (1977); Monzon et al. (2021)). During that period, named "critical period for yield", in the absence of nutrient and water restriction, variations in accumulated solar radiation during pod setting are closely associated with changes in the number of grains per unit area (Calviño et al., 2003; Kantolic and Slafer, 2001; Nico et al., 2015). Additionally, during that critical period the variations in the number of grains per unit area are mostly associated with variations in the number of pods per unit area (Jiang and Egli, 1995; Monzon et al., 2021; Nico et al., 2019). As overlapping between grain number and grain weight determination is common in soybean, the environmental conditions at which the critical period is exposed determine not only the number of grains but also grain weight and thereby final yield (Monzon et al., 2021). A positive relationship has been found between the duration of the critical period and yield (Dunphy et al., 1979), as well as between yield and the seed number per unit area (Egli and Bruening, 2000; Kantolic and Slafer, 2007). Therefore, delays in sowing date have a negative impact on yield because they generally expose the critical period to less favourable growing conditions, such as shorter days and reduced incident radiation as well as temperature (Egli and Bruening, 2000; Kantolic et al., 2013; Nico et al., 2015). At the light of evidences described above in terms of the importance of the environmental conditions during the "critical period" for soybean's yield determination, accurate prediction of its occurrence is important for assisting farmers on the genotype and sowing date selection.

Simulation models like APSIM (Keating et al., 2003) and DSSAT (Jones et al., 2003) are extremely useful to predict crop phenology and seed yield under different environments. However, in these models the calibration of genetic coefficients for simulating phenology and yield is a complex and time-consuming process limiting the number of genotypes available for simulation. Consequently, the modelled genotypes may not be representative of the broad range of genetic material grown by farmers, limiting the scope of the tool for farmer management decisions. To tackle this issue in a simple way, simulation models use generic coefficients based on maturity groups and growth habits (Salmerón and Purcell, 2016).

Here we aimed at constructing a model, named CRONOSOJA, simple enough to be calibrated for many varieties available at the market, yet able to predict phenology with reasonable accuracy across Argentina, Paraguay and Uruguay. We aimed at (i) characterising the genotypic variability of phenology within the current commercial soybean varieties of Argentina, Uruguay and Paraguay, and (ii) building a simple dynamic model based on photothermal conditions of different regions to predict different phenological stages in soybean. The model outputs are currently

available — in Spanish language — on an interactive website (http://cronosoja.agro.uba.ar/index.php/), which also includes estimates of frost risk and water availability during the growing season.

2 Materials and Methods

2.1 Sites, field experiments and genotypes

Forty-three field experiments were established in Argentina, Paraguay, and Uruguay, from 2016 to 2020 (Figure 1, Table 1). Each experiment consisted of 34 soybean varieties of different maturity groups (MG) from 2 to 6, representing some of the most frequently sown varieties in these countries (Table 2). In order to explore a wide range of temperature and photoperiod conditions, experiments were sown from the middle of October to the end of January, with a gap of around one month between successive sowing dates at different locations (Table 1). Weeds, insects, and diseases were controlled to ensure optimal growing conditions.

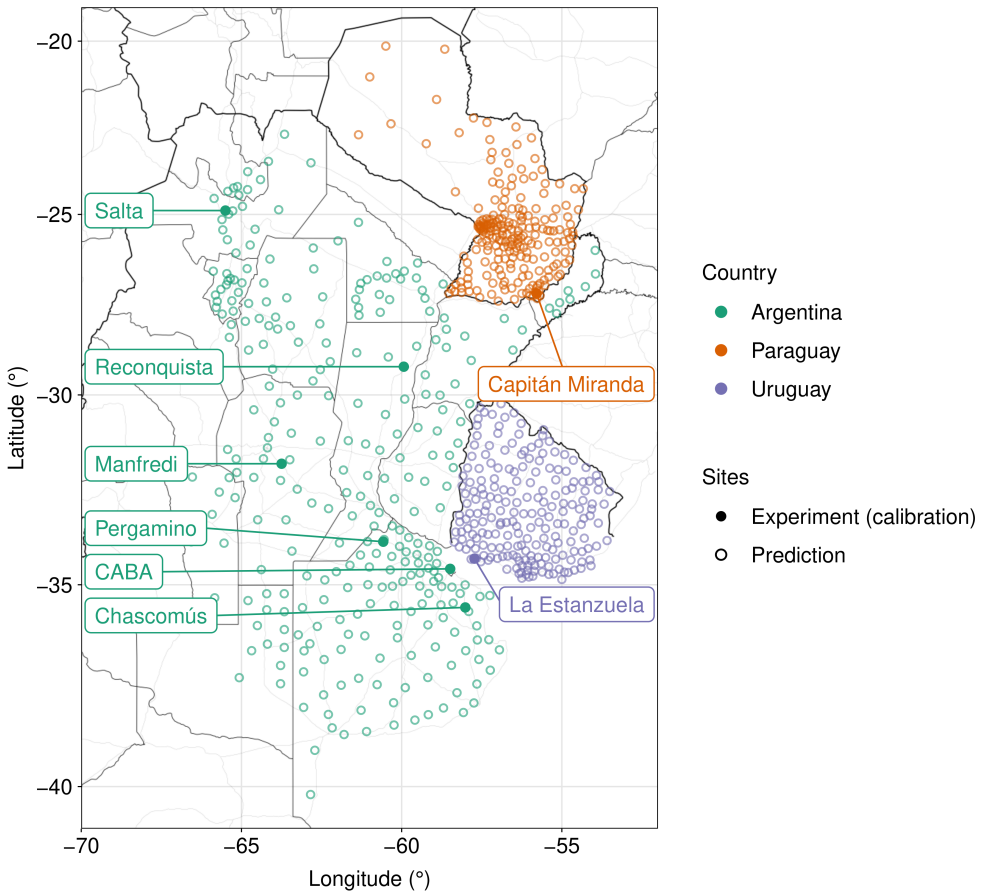

Figure 1: Distribution of experimental sites (solid symbols) and prediction sites (empty symbols) across Argentina, Paraguay and Uruguay.

Table 1: The location of experimental sites, and sowing dates tested in each of the four experimental seasons.

Country	Site	Latitude (°)	Longitude (°)	2016/17	2017/18	2018/19	2019/20	2020/21
Argentina	CABA	-34.59199	-58.48499		23 Mar			

Country	Site	Latitude (°)	Longitude (°)	2016/17	2017/18	2018/19	2019/20	2020/21
	Chascomús	-35.57856	-58.01384	14 Oct				
				22 Nov				
				23 Dec				
	Manfredi	-31.84479	-63.74709		13 Nov			
					14 Dec			
						29 Oct		
						03 Dec		
						16 Jan		
							22 Jan	
	Pergamino	-33.89127	-60.57459	16 Oct				
				18 Nov				
				15 Dec				
					10 Nov			
					15 Dec			
					11 Jan			
						09 Oct		
						21 Dec		
						10 Jan		
	Reconquista	-29.23329	-59.93329	31 Oct				
				25 Nov				
					06 Dec			
					02 Jan			
					25 Jan			
						09 Nov		
						27 Dec		
						04 Jan		
						21 Mar		
							30 Jan	
	Salta	-24.88999	-65.49999			30 Nov		
							04 Jan	
							29 Jan	
Paraguay	Capitán Miranda	-27.22186	-55.78824			12 Dec		
							22 Nov	
							23 Dec	
								15 Jan
Uruguay	La Estanzuela	-34.32940	-57.72880		14 Nov			
					08 Dec			
					28 Dec			
						18 Oct		
						20 Nov		
						26 Dec		
							14 Jan	

At each experimental site, the 34 genotypes detailed in Table 2 were sown simultaneously in a wide range of sowing dates in field plots of 4 rows wide and 5 m long with a density of ca. 25 pl m^{-2} (early sowings) and ca. 30 pl m^{-2} (late sowings) under no water and nutritional restrictions. The experimental design was a randomised complete block design with three repetitions per genotype. Different phenological stages were recorded at least thrice weekly, plot by plot, by using the scale of Fehr and Caviness (1977) (see Table 3).

Environmental data collected included daily minimum and maximum temperature (°C) and photoperiod length (h). At the locations where weather stations were available, these data were recorded *in situ*, close to the experiments.

At locations where weather stations were not available, or when there were temporal gaps in the data, we used data from Hersbach et al. (2018), downloaded from the Copernicus Climate Change Service (C3S) Climate Data Store. These gridded data were processed to extract temperature values from the exact coordinates of each site by means of bi-cubic interpolation with the software CDO (Schulzweida, 2021). Daily minimum and maximum temperatures were determined from hourly temperatures. Photoperiod was estimated given the site latitude and date with the package `geosphere` (Hijmans, 2021) in R (R Core Team, 2022).

Table 2: Genotypes used in field experiments, including their maturity group (MG) and breeding company.

MG	Company	Genotype
2.5	GDM	DM 2200
2.5	Nidera	NS 2632
3.0	Nidera	NS 3220
3.5	GDM	DM 3312
3.5	Nidera	NS 3809
3.7	Ferias del Norte	FN 3.85
3.9	Santa Rosa Semillas	RA 349
4.0	GDM	DM 3815
4.0	GDM	DM 40R16
4.1	Ferias del Norte	FN 4.35
4.2	Asgrow	AW 4326
4.5	GDM	DM 4612
4.7	Bayer	CZ 4505
4.9	Bayer	CZ 4.97
4.9	Nidera	NS 4955
5.0	GDM	DM 50i17
5.1	Nidera	NS 5258
5.5	GDM	DM 53i53
5.5	INIA Uruguay	Génesis 5501
5.5	INTA	INTA Paraná 5500
5.5	Santa Rosa Semillas	RA 550
5.6	INIA Uruguay	Génesis 5601
5.6	INIA Uruguay	Génesis 5602
5.7	Asgrow	AW 5714
5.7	Asgrow	AW 5815
5.7	Bayer	CZ 5905
5.9	Santa Rosa Semillas	RA 549
6.0	GDM	DM 6.2i
6.2	INIA Uruguay	Génesis 6201
6.2	INTA	INTA Paraná 6200
6.3	Bayer	CZ 6505
6.5	Asgrow	AW M6410
6.5	Nidera	NS 6248
6.8	Santa Rosa Semillas	RA 655

2.2 Formulating a daily time-step developmental model

The phenological scale of Fehr and Caviness (1977) was translated into a numeric scale to be used as a regression dependent variable called R (Table 3).

Table 3: Translation of the scale of Fehr and Caviness (1977) into a numeric variable (R).

Stage	Abbreviation	R
Sowing	SO	0
Emergence	EM	1
End of juvenile	JU	2
Floral initiation	R0	3
Flowering	R1	4
Start pod	R3	5
Start seed filling	R5	6
Maximum seed size	R6	7
Physiological maturity	R7	8
Harvest maturity	R8	9

We formulated a multiplicative model to calculate the development rate depending on daily photoperiod and temperature (Grimm et al., 1994; Major et al., 1975b). The equation describing the developmental stage (R) at a specified time (t, in days after sowing) at site i and genotype j was

$$R_{ijt} = \begin{cases} R_{ijt-1} + \frac{1}{D_{\text{SO-EM}}}\phi_{T_{ijt}}, & \text{if } R_{ijt-1} < 1 \\ R_{ijt-1} + \frac{1}{D_{\text{EM-JU}}}\phi_{T_{ijt}}, & \text{if } 1 \leq R_{ijt-1} < 2 \\ R_{ijt-1} + \frac{1}{D_{\text{JU-R0}}}\phi_{T_{ijt}}\phi_{P_{ijt}}, & \text{if } 2 \leq R_{ijt-1} < 3 \\ R_{ijt-1} + \frac{1}{D_{\text{R0-R1}_j}}\phi_{T_{ijt}}\phi_{P_{ijt}}, & \text{if } 3 \leq R_{ijt-1} < 4 \\ R_{ijt-1} + \frac{1}{D_{\text{R1-R3}_j}}\phi_{T_{ijt}}\phi_{P_{ijt}}, & \text{if } 4 \leq R_{ijt-1} < 5 \\ R_{ijt-1} + \frac{1}{D_{\text{R3-R5}_j}}\phi_{T_{ijt}}\phi_{P_{ijt}}, & \text{if } 5 \leq R_{ijt-1} < 6 \\ R_{ijt-1} + \frac{1}{D_{\text{R5-R6}_j}}\phi_{T_{ijt}}\phi_{P_{ijt}}, & \text{if } 6 \leq R_{ijt-1} < 7 \\ R_{ijt-1} + \frac{1}{D_{\text{R6-R7}_j}}\phi_{T_{ijt}}\phi_{P_{ijt}}, & \text{if } 7 \leq R_{ijt-1} < 8 \\ R_{ijt-1} + \frac{1}{D_{\text{R7-R8}_j}}, & \text{otherwise} \end{cases} \tag{1}$$

where R_{ijt-1} is the developmental stage from the previous day ($t-1$) at site i and genotype j; $D_{\text{SO-EM}}$ and $D_{\text{EM-JU}}$ are thermal days (i.e., equivalent to calendar days if temperature is optimum) for phases SO-EM and EM-JU, respectively; $D_{\text{JU-R0}}$, $D_{\text{R0-R1}}$, $D_{\text{R1-R3}}$, $D_{\text{R3-R5}}$, $D_{\text{R5-R6}}$, $D_{\text{R6-R7}}$, are photothermal days (i.e., equivalent to calendar days if temperature is optimum and photoperiod is less or equal to the optimum) for stages JU-R0, R0-R1, R1-R3, R3-R5, R5-R6, and R6-R7, respectively; and $D_{\text{R7-R8}}$ are days for stage R7-R8. On the other hand, $\phi_{T_{ijt}}$ and $\phi_{P_{ijt}}$ are multipliers that describe the temperature and photoperiod responses, respectively, by adopting values between 0 and 1. Therefore, $\phi_{T_{ijt}}$ and $\phi_{P_{ijt}}$ penalise the maximum developmental rates (e.g. $1/D_{\text{R1-R3}}$). $\phi_{T_{ijt}}$ and $\phi_{P_{ijt}}$ are defined for site i, genotype j and day t, that is, these functions depend on the site because of its input variables and depend on the genotype because of its genotype-specific parameters.

For simulating the response of $\phi_{T_{ijt}}$ to temperature we used the function of Wang and Engel (1998),

$$\alpha = \frac{log(2)}{log(\frac{T_{\text{m}}-T_{\text{b}}}{T_{\text{o}}-T_{\text{b}}})} \tag{2}$$

$$\phi_{T_{ijt}} = \begin{cases} \frac{2(X_{T_{it}}-T_{\text{b}})^{\alpha}(T_{\text{o}}-T_{\text{b}})^{\alpha}-(X_{T_{it}}-T_{\text{b}})^{2\alpha}}{(T_{\text{o}}-T_{\text{b}})^{2\alpha}}, & \text{if } T_{\text{b}} \leq X_{T_{it}} \leq T_{\text{m}} \\ 0, & \text{otherwise} \end{cases} \tag{3}$$

where $X_{T_{it}}$ is daily air temperature of site i and day t, T_{b} is the base temperature, T_{o} is the optimum temperature, and T_{m} is the maximum temperature, all in °C.

At this stage, the first alternative models were evaluated: one where T_b was constant across developmental phases, and another one where it differed between developmental stage ranges, so that

$$T_\mathrm{b} = \begin{cases} T_{\mathrm{b_{SO\text{-}R1}}}, & \text{if } R_{ijt-1} < 4 \\ T_{\mathrm{b_{R1\text{-}R5}}}, & \text{if } 4 \leq R_{ijt-1} < 6 \\ T_{\mathrm{b_{R5\text{-}R7}}}, & \text{otherwise.} \end{cases} \tag{4}$$

The temperature function was calculated sub-daily, at 3-hour intervals, by interpolating between daily minimum and daily maximum temperatures (Jones et al., 1986) using a cubic function as employed in APSIM (Keating et al., 2003). The resulting eight, sub-daily temperature multipliers were averaged to represent a daily temperature multiplier $\phi_{T_{ijt}}$.

We wanted to test competing models at this stage, since current models differ in their structure. For instance, DSSAT includes a parameter named R1PPO, which increases photoperiod sensitivity after R1 by reducing the optimum photoperiod by an amount that depends on the genotype. APSIM, however, lacks this parameter. Thus, we tested the alternative of including or excluding ΔP_o, leading to four alternative models (Table 5).

For formalising the photoperiod multiplier, $\phi_{P_{ijt}}$, we formulated the second set of alternative equations: one where the photoperiod response was constant across reproductive development, and another one where the response threshold was reduced by the parameter ΔP_{o_j} (similar to parameter R1PPO in CROPGRO (Boote et al., 1998b)), making plants more sensitive to photoperiod after R1. Therefore, the simpler model for the photoperiod multiplier was

$$\phi_{P_{ijt}} = \begin{cases} 1, & \text{if } X_{P_{it}} \leq P_{\mathrm{o}_j} \\ 1 - P_{\mathrm{s}_j}(X_{P_{it}} - P_{\mathrm{o}_j}), & \text{if } X_{P_{it}} > P_{\mathrm{o}_j} \end{cases} \tag{5}$$

whereas the more complex one was

$$\phi_{P_{ijt}} = \begin{cases} 1, & \text{if } X_{P_{it}} \leq P_{\mathrm{o}_j}, R_{ijt-1} < 4 \\ 1, & \text{if } X_{P_{it}} \leq (P_{\mathrm{o}_j} - \Delta P_{\mathrm{o}_j}), R_{ijt-1} \geq 4 \\ 1 - P_{\mathrm{s}_j}(X_{P_{it}} - P_{\mathrm{o}_j}), & \text{if } X_{P_{it}} > P_{\mathrm{o}_j}, R_{ijt-1} < 4 \\ 1 - P_{\mathrm{s}_j}(X_{P_{it}} - P_{\mathrm{o}_j} - \Delta P_{\mathrm{o}_j}), & \text{if } X_{P_{it}} > (P_{\mathrm{o}_j} - \Delta P_{\mathrm{o}_j}), R_{ijt-1} \geq 4 \end{cases} \tag{6}$$

where $X_{P_{it}}$ is the photoperiod (h) of site i and day t, P_{o_j} is the optimum photoperiod of genotype j, P_{s_j} is the photoperiod sensitivity of genotype j, and ΔP_{o_j} represents the shift in the optimum photoperiod after R1 of genotype j.

2.3 Explaining initial variability in phenology

To understand the sources of variation affecting the duration of each developmental stage, we fitted a mixed effects regression explaining the duration of stages as a function of sowing date (days since 1st October of the current year), maturity group (as factor), genotype, site and year. Fixed effects were the effect of sowing date, maturity group and, when significant, their interaction. Random effects (random intercepts) were genotype, site and year. Models were fitted with package `lme4` (Bates et al., 2015) in R. Models with and without an interaction between sowing date and maturity group were compared by means of Akaike information criteria (AIC). The resulting best models included the interaction term for stages EM-R1, R1-R3, R3-R5, and R5-R6 (Equation 7), but lacked this term for stages R6-R7 and R7-R8 (Equation 8):

$$Y_{ijklm} = (\beta_0 + u_{0j} + v_{0k} + w_{0l}) + \beta_\mathrm{SD} X_{\mathrm{SD}_{ijklm}} + \beta_{\mathrm{MG}_i} X_{\mathrm{MG}_i} + \beta_{\mathrm{SD,MG}_i} X_{\mathrm{SD}_{ijklm}} X_{\mathrm{MG}_i} + \epsilon_{ijklm} \tag{7}$$

$$Y_{ijklm} = (\beta_0 + u_{0j} + v_{0k} + w_{0l}) + \beta_\mathrm{SD} X_{\mathrm{SD}_{ijklm}} + \beta_{\mathrm{MG}_i} X_{\mathrm{MG}_i} + \epsilon_{ijklm} \tag{8}$$

where Y_{ijklm} is the duration of the stage for maturity group i, genotype j, site k, year l and replicate m; β_0 is the general intercept; β_{SD} is the slope against sowing date; $X_{\text{SD}_{ijklm}}$ is the sowing date (as days since 1st October) of maturity group i, genotype j, site k, year l and replicate m; β_{MG_i} is the effect of maturity group i; X_{MG_i} is maturity group i; $\beta_{\text{SD,MG}_i}$ is the effect of the interaction between sowing date and maturity group i; u_{0j} is the random effect of genotype j; v_{0k} is the random effect of site k; w_{0l} is the random effect of year l; and ϵ_{ijklm} is the error of maturity group i, genotype j, site k, year l and replicate m.

Once the appropriate models were fitted, we obtained the variance of each source of variation with the function `get_variances` from the `R` package `insight` (Lüdecke et al., 2019). Since this resulted in a combined fixed effects variance (i.e. sowing date and maturity group variances were amalgamated, rendering them indistinguishable from one another), we further partitioned the fixed effects variance per source of variation using the `R` package `partR2` (Stoffel et al., 2020).

2.4 Fitting one model per genotype (genotype-based model)

The first step of the calibration was performed in a genotype-based manner. Parameters to be calibrated were photothermal days $D_{\text{R0-R1}}$, $D_{\text{R1-R3}}$, $D_{\text{R3-R5}}$, $D_{\text{R5-R6}}$, $D_{\text{R6-R7}}$, calendar days $D_{\text{R7-R8}}$, and those parameters contained in the temperature function $\phi_{T_{ijt}}$ and in the photoperiod response function $\phi_{P_{ijt}}$. From $\phi_{T_{ijt}}$, we chose to calibrate the base temperature T_{b}, as judging from the literature was the parameter that changed the most (Jones et al., 1986; Setiyono et al., 2007). Parameters T_{o} and T_{m} were set to 30 and 45 °C, respectively. From $\phi_{P_{ijt}}$, we calibrated all three parameters, that is, P_{o}, P_{s}, and, where present, ΔP_{o}.

To perform the calibration, we coded a likelihood function in the hybrid language `Rcpp` (Eddelbuettel and François, 2011). This function ran the model per genotype, across all sowing dates and locations where the corresponding genotype was sown, iterating through possible solutions of $D_{\text{R0-R1}}$, $D_{\text{R1-R3}}$, $D_{\text{R3-R5}}$, $D_{\text{R5-R6}}$, $D_{\text{R6-R7}}$, $D_{\text{R7-R8}}$, T_{b}, P_{o}, P_{s}, and ΔP_{o}. The function returned a log-likelihood value that was maximised by means of a Metropolis-Hastings Markov Chain Monte Carlo (MCMC) implemented in the `R` package `BayesianTools` (Hartig et al., 2019). The MCMC was performed in four independent chains with 3×10^5 iterations, which ensured that the chains mixed appropriately. Convergence was assured by the diagnostic $\widehat{R}$, which was always less than 1.01 (Vehtari et al., 2021).

The prior distributions of most parameters were constructed by sampling from the literature, with the following modifications. First, their standard deviation was tripled to allow the model to explore other possible values given our different model structure. Second, in the case of T_{b}, as we were implementing a different function than those used in Jones et al. (1986), Archontoulis et al. (2014) or Setiyono et al. (2007), we set them to have mean zero and a large standard deviation, since the actual values were unknown. Third, in the case of $D_{\text{R3-R5}}$, their mean was calculated by subtracting from DSSAT parameter `FL.SD` (photothermal days from R1 to R5, Jones et al. (1986)) the parameter `FL.SH`, the latter being equivalent to $D_{\text{R1-R3}}$. All priors were specified as truncated normal distributions with function `createTruncatedNormalPrior` from `BayesianTools`. Their final means, standard deviations, lower and upper limits are shown in Table 4. No priors were constructed for parameters $D_{\text{SO-EM}}$, $D_{\text{EM-JU}}$ and $D_{\text{JU-R0}}$, which were given values 5, 5, and 6 thermal days, respectively, after consulting parameters from APSIM (presented by Archontoulis et al. (2014)).

Table 4: Mean, standard deviation, lower and upper limits for the truncated normal priors of each genotype-based model parameter.

Parameter	Mean	Standard deviation	Lower limit	Upper limit
$T_{\text{b}_{\text{SO-R1}}}$ (°C)	0.00	3.00	-1000.0	10.0
$T_{\text{b}_{\text{R1-R5}}}$ (°C)	0.00	3.00	-1000.0	10.0
$T_{\text{b}_{\text{R5-R7}}}$ (°C)	0.00	30.00	-1000.0	10.0
$D_{\text{R0-R1}}$ (d)	6.00	9.00	1.0	30.0
$D_{\text{R1-R3}}$ (d)	7.50	4.00	1.0	30.0
$D_{\text{R3-R5}}$ (d)	7.63	2.00	1.0	30.0
$D_{\text{R5-R6}}$ (d)	13.70	10.00	1.0	40.0

Parameter	Mean	Standard deviation	Lower limit	Upper limit
$D_{\text{R6-R7}}$ (d)	13.70	10.00	1.0	40.0
$D_{\text{R7-R8}}$ (d)	12.00	3.00	1.0	30.0
P_{o} (h)	13.30	1.00	10.0	16.0
P_{s} (h^{-1})	0.29	0.03	0.0	0.6
ΔP_{o} (h)	0.00	0.40	-1.0	1.0

For model selection, we followed a multi-model inference approach to select the best models based on information criteria (Garibaldi et al., 2017). In each case, the most parsimonious model was chosen based on information criteria inferred by approximate leave-one-out cross-validation (LOO) with package `loo` (Vehtari et al., 2019) for R, which implements a fast computation of LOO using Pareto smoothed importance-sampling (PSIS-LOO, Vehtari et al. (2017)). For this, a second `Rcpp` function was coded that instead of yielding a cumulative log-likelihood resulted in a point-wise log-likelihood, i.e. a log-likelihood matrix with rows equal to the number of observations and columns equal to the number of iterations. The number of iterations was obtained from concatenating the four chains, discarding the burn-in fraction, and thinning every 60 iterations. The appropriate values of thinning were found after performing an autocorrelation test with the R package `coda` (Plummer et al., 2006). This point-wise log-likelihood was fed into the function `loo` from the package of the same name (Vehtari et al., 2019). Leave-one-out cross-validation, as implemented in the package `loo`, allowed us to calculate an expected log point-wise predictive density (ELPD). This per-genotype ELPD was concatenated into one vector (representing all genotypes) per each of the four competing models so that a combined ELPD per model was obtained. With these ELPDs, models were compared both by pseudo-Bayesian model averaging and by stacking (Yao et al., 2017), obtaining a probability (weight) per model. The model with the highest weight is the best model, that is, the one with best predictive accuracy and likely the one that fits the data best with the least amount of parameters. These are shown in Table 5.

2.5 Generating a common hierarchical model across genotypes

At the second stage of the calibration, we wanted to unify all 34 genotype-based models into one hierarchical model across maturity groups and genotypes. To do so we constructed a Bayesian multivariate regression that simultaneously predicted the parameters of the aforementioned best model using maturity group (MG) as a covariate. The model was multivariate in the sense that parameters $D_{\text{R0-R1}}$, $D_{\text{R1-R3}}$, $D_{\text{R3-R5}}$, $D_{\text{R5-R6}}$, $D_{\text{R6-R7}}$, $D_{\text{R7-R8}}$, T_{b}, P_{o} , P_{s} , and ΔP_{o}, were regressed simultaneously. The model was in turn a mixed-effects linear model, with MG as a fixed effect and genotype as a random effect (random intercepts). This model can be represented as

$$D_{\text{R0-R1}_{ij}} = (\beta_0^{D_{\text{R0-R1}}} + b_{0j}^{D_{\text{R0-R1}}}) + \beta_{\text{MG}}^{D_{\text{R0-R1}}} X_{\text{MG}_j} + \epsilon_{ij}^{D_{\text{R0-R1}}} \tag{9}$$

$$D_{\text{R1-R3}_{ij}} = (\beta_0^{D_{\text{R1-R3}}} + b_{0j}^{D_{\text{R1-R3}}}) + \beta_{\text{MG}}^{D_{\text{R1-R3}}} X_{\text{MG}_j} + \epsilon_{ij}^{D_{\text{R1-R3}}} \tag{10}$$

$$D_{\text{R3-R5}_{ij}} = (\beta_0^{D_{\text{R3-R5}}} + b_{0j}^{D_{\text{R3-R5}}}) + \beta_{\text{MG}}^{D_{\text{R3-R5}}} X_{\text{MG}_j} + \epsilon_{ij}^{D_{\text{R3-R5}}} \tag{11}$$

$$D_{\text{R5-R6}_{ij}} = (\beta_0^{D_{\text{R5-R6}}} + b_{0j}^{D_{\text{R5-R6}}}) + \beta_{\text{MG}}^{D_{\text{R5-R6}}} X_{\text{MG}_j} + \epsilon_{ij}^{D_{\text{R5-R6}}} \tag{12}$$

$$D_{\text{R6-R7}_{ij}} = (\beta_0^{D_{\text{R6-R7}}} + b_{0j}^{D_{\text{R6-R7}}}) + \beta_{\text{MG}}^{D_{\text{R6-R7}}} X_{\text{MG}_j} + \epsilon_{ij}^{D_{\text{R6-R7}}} \tag{13}$$

$$D_{\text{R7-R8}_{ij}} = (\beta_0^{D_{\text{R7-R8}}} + b_{0j}^{D_{\text{R7-R8}}}) + \beta_{\text{MG}}^{D_{\text{R7-R8}}} X_{\text{MG}_j} + \epsilon_{ij}^{D_{\text{R7-R8}}} \tag{14}$$

$$T_{\text{b}_{\text{SO-R1}}ij} = (\beta_0^{T_{\text{b}_{\text{SO-R1}}}} + b_{0j}^{T_{\text{b}_{\text{SO-R1}}}}) + \beta_{\text{MG}}^{T_{\text{b}_{\text{SO-R1}}}} X_{\text{MG}_j} + \epsilon_{ij}^{T_{\text{b}_{\text{SO-R1}}}} \tag{15}$$

$$T_{\text{b}_{\text{R1-R5}}ij} = (\beta_0^{T_{\text{b}_{\text{R1-R5}}}} + b_{0j}^{T_{\text{b}_{\text{R1-R5}}}}) + \beta_{\text{MG}}^{T_{\text{b}_{\text{R1-R5}}}} X_{\text{MG}_j} + \epsilon_{ij}^{T_{\text{b}_{\text{R1-R5}}}} \tag{16}$$

$$T_{\text{b}_{\text{R5-R7}}ij} = (\beta_0^{T_{\text{b}_{\text{R5-R7}}}} + b_{0j}^{T_{\text{b}_{\text{R5-R7}}}}) + \beta_{\text{MG}}^{T_{\text{b}_{\text{R5-R7}}}} X_{\text{MG}_j} + \epsilon_{ij}^{T_{\text{b}_{\text{R5-R7}}}} \tag{17}$$

$$P_{\text{o}_{ij}} = (\beta_0^{P_{\text{o}}} + b_{0j}^{P_{\text{o}}}) + \beta_{\text{MG}}^{P_{\text{o}}} X_{\text{MG}_j} + \epsilon_{ij}^{P_{\text{o}}} \tag{18}$$

$$P_{\text{s}_{ij}} = (\beta_0^{P_{\text{s}}} + b_{0j}^{P_{\text{s}}}) + \beta_{\text{MG}}^{P_{\text{s}}} X_{\text{MG}_j} + \epsilon_{ij}^{P_{\text{s}}} \tag{19}$$

$$\Delta P_{\text{o}_{ij}} = (\beta_0^{\Delta P_{\text{o}}} + b_{0j}^{\Delta P_{\text{o}}}) + \beta_{\text{MG}}^{\Delta P_{\text{o}}} X_{\text{MG}_j} + \epsilon_{ij}^{\Delta P_{\text{o}}} \tag{20}$$

where $D_{\text{R0-R1}_{ij}}$ is the i draw from parameter $D_{\text{R0-R1}}$ of genotype j; $\beta_0^{D_{\text{R0-R1}}}$ is the global intercept and $\beta_1^{D_{\text{R0-R1}}}$ the slope of the regression against X_{MG_j}, which represents maturity group from genotype j; and $b_{0j}^{D_{\text{R0-R1}}}$ and $\epsilon_{ij}^{D_{\text{R0-R1}}}$ are random variables representing, respectively, the random intercept of genotype j, and the random error from draw i and genotype j. The same nomenclature applies to the rest of the response variables.

Random effects of genotypes and errors were drawn from multivariate normal distributions (MVN) with mean 0 and variance-covariance matrices $\mathbf{\Sigma}_b$ and $\mathbf{\Sigma}_\epsilon$. In the case of random intercepts resulting from genotypes, b_{0j}, these were

$$\begin{bmatrix} b_{0j}^{D_{\text{R0-R1}}} \\ b_{0j}^{D_{\text{R1-R3}}} \\ b_{0j}^{D_{\text{R3-R5}}} \\ b_{0j}^{D_{\text{R5-R6}}} \\ b_{0j}^{D_{\text{R6-R7}}} \\ b_{0j}^{D_{\text{R7-R8}}} \\ b_{0j}^{T_{\text{b}_{\text{SO-R1}}}} \\ b_{0j}^{T_{\text{b}_{\text{R1-R5}}}} \\ b_{0j}^{T_{\text{b}_{\text{R5-R7}}}} \\ b_{0j}^{P_{\text{o}}} \\ b_{0j}^{P_{\text{s}}} \\ b_{0j}^{\Delta P_{\text{o}}} \end{bmatrix} \sim \text{MVN}(0, \mathbf{\Sigma}_b) \tag{21}$$

where $b_{0j}^{D_{\text{R0-R1}}}$, $b_{0j}^{D_{\text{R1-R3}}}$, $b_{0j}^{D_{\text{R3-R5}}}$, $b_{0j}^{D_{\text{R5-R6}}}$, $b_{0j}^{D_{\text{R6-R7}}}$, $b_{0j}^{D_{\text{R7-R8}}}$, $b_{0j}^{T_{\text{b}_{\text{SO-R1}}}}$, $b_{0j}^{T_{\text{b}_{\text{R1-R5}}}}$, $b_{0j}^{T_{\text{b}_{\text{R5-R7}}}}$, $b_{0j}^{P_{\text{o}}}$, $b_{0j}^{P_{\text{s}}}$ and $b_{0j}^{\Delta P_{\text{o}}}$ are the random effects of genotype j over parameters $D_{\text{R0-R1}}$, $D_{\text{R1-R3}}$, $D_{\text{R3-R5}}$, $D_{\text{R5-R6}}$, $D_{\text{R6-R7}}$, $D_{\text{R7-R8}}$, $T_{\text{b}_{\text{SO-R1}}}$, $T_{\text{b}_{\text{R1-R5}}}$, $T_{\text{b}_{\text{R5-R7}}}$, P_{o}, P_{s} and ΔP_{o}, respectively, and $\mathbf{\Sigma}_b$ is their variance-covariance matrix, with diagonal elements $\sigma^2_{b_0^{D_{\text{R0-R1}}}}$, $\sigma^2_{b_0^{D_{\text{R1-R3}}}}$, $\sigma^2_{b_0^{D_{\text{R3-R5}}}}$, $\sigma^2_{b_0^{D_{\text{R5-R6}}}}$, $\sigma^2_{b_0^{D_{\text{R6-R7}}}}$, $\sigma^2_{b_0^{D_{\text{R7-R8}}}}$, $\sigma^2_{b_0^{T_{\text{b}_{\text{SO-R1}}}}}$, $\sigma^2_{b_0^{T_{\text{b}_{\text{R1-R5}}}}}$, $\sigma^2_{b_0^{T_{\text{b}_{\text{R5-R7}}}}}$, $\sigma^2_{b_0^{P_{\text{o}}}}$, $\sigma^2_{b_0^{P_{\text{s}}}}$ and $\sigma^2_{b_0^{\Delta P_{\text{o}}}}$ showing the genotype variances and off-diagonal elements showing their covariances between different parameters (Section 9, Equation 36).

Errors ϵ_{ij} are correlated between parameters as well, so that

$$\begin{bmatrix} \epsilon_{ij}^{D_{\text{R0-R1}}} \\ \epsilon_{ij}^{D_{\text{R1-R3}}} \\ \epsilon_{ij}^{D_{\text{R3-R5}}} \\ \epsilon_{ij}^{D_{\text{R5-R6}}} \\ \epsilon_{ij}^{D_{\text{R6-R7}}} \\ \epsilon_{ij}^{D_{\text{R7-R8}}} \\ \epsilon_{ij}^{T_{\text{b}_{\text{SO-R1}}}} \\ \epsilon_{ij}^{T_{\text{b}_{\text{R1-R5}}}} \\ \epsilon_{ij}^{T_{\text{b}_{\text{R5-R7}}}} \\ \epsilon_{ij}^{P_{\text{o}}} \\ \epsilon_{ij}^{P_{\text{s}}} \\ \epsilon_{ij}^{\Delta P_{\text{o}}} \end{bmatrix} \sim \text{MVN}(0, \mathbf{\Sigma}_\epsilon) \tag{22}$$

where $\mathbf{\Sigma}_\epsilon$ is their variance covariance matrix, with its diagonal elements capturing the variances of the residuals of each response variable, and its off-diagonal elements representing the covariances between residuals of different response variables (Section 9, Equation 37).

During this stage of the calibration, the multivariate models were fitted with the probabilistic programming language `Stan` (Carpenter et al., 2017), accessed through package `brms` (Bürkner, 2018) in `R`. For fitting these models, the

MCMC was run in 4 chains, where each chain had 2000 iterations, and the first 1000 were removed as part of the warm-up process, resulting in an MCMC sample of 4000 values. We used the default priors defined in the function `brm` from package `brms` (see Severini et al. (2020) for a detailed description). Convergence of the posterior density was evaluated again by the $\widehat{R}$ test statistic, where values less than 1.01 indicated that the MCMC sampling process was adequate (Vehtari et al., 2021).

Given that ten model parameters were regressed simultaneously, there were competing models at this stage too, where parameters were allowed to be a function, or not, of MG. Several alternative models, possessing different parameters' response to MG, were compared again using LOO by obtaining a probability (weight) per model (Vehtari et al., 2019).

Fixed and random effects are reported always as the median and its 90% credible-interval bounds (CI: lower limit, upper limit) of the posterior distribution.

2.6 Calibration and validation data sets

In order to have data both for calibrating the model as well as for testing it, we split the experimental data randomly within each genotype (i.e. a single genotype could contain multiple combinations of locations and sowing dates) into calibration (75%) and validation (25%) data sets with the function `initial_split` from the `R` package `rsample` (Silge et al., 2021). All subsequent calibrations, both genotype by genotype as well as the unified, hierarchical model, were done with the calibration data set. Data from the testing split were used to compare observed days after sowing (DAS) to R1, R3, R5, R6, R7 and R8 with the simulated DAS of each stage. This comparison was made by means of root mean squared error (RMSE), relative RMSE (RRMSE) and relative lack of accuracy (RLA) using the `R` package `metrica` (Correndo et al., 2021) from R. RLA measures the percentage of error given by how much a symmetric regression line (SMA) departs from the 1:1 line, representing systematic error (Correndo et al., 2021), in contrast with the relative lack of precision representing unsystematic error which can be visualised as random error around the SMA.

2.7 Predictions for website deployment

After calibrating the model and validating it against the validation dataset, the last step a was to generate predictions that served as inputs of the website. First, the main soybean producing regions of each country were identified after consulting local government public databases. Then, shapefiles for each country were downloaded from https://gadm.org/download_country_v3.html and one coordinate per province-district combination was calculated as a centroid of its shapefile polygon with package `sf` (Pebesma, 2018) in `R` (Figure 1). For every centroid coordinate, daily maximum and minimum temperatures for the last 10 years as well as daily photoperiod were determined in the same way as the calibration weather data processing detailed in Section 2.1. Sowing dates were simulated for every day from the beginning of October to the end of January for 10 years. For every sowing date day-of-year, genotype and location, days after sowing were averaged across 10 years for stages R1, R3, R5, R6, R7 and R8. These averages were later saved as CSV spreadsheets on a prediction-site basis to feed the website.

2.8 Available soil water estimation

To describe the temporal dynamics of available soil water, we used a soil water balance simulation model BHOA (for its acronym in Spanish: "Balance Hidrológico Operativo para el Agro"; Fernández-Long et al. (2013)). The BHOA is a one-layer bucket model that establishes a balance a balance between the atmospheric demand of water (given by the potential evapotranspiration; PET), the supply of water (given by the precipitation; PP) and the water stored in the ground (soil moisture; SM)

$$\mathrm{SM}_t = \mathrm{SM}_{t-1} e^{\frac{\mathrm{PP - PET}}{\mathrm{FC - DL}}} \tag{23}$$

where SM_t is the soil moisture on day t, SM_{t-1} is the soil moisture on the day before, FC is the field capacity and DL is the drying limit, calculated as a percentage of the permanent wilting point (PWP). The available soil water is the difference between the amount of SM_t and the amount of PWP. This model has been proven to have a very good fit with observed data (Fernández-Long et al., 2018; Spennemann et al., 2020) and has been used in Argentina for the estimation of soil moisture with different objectives (Fernández-Long et al., 2021; Penalba et al., 2019; Peretti et al., 2023; Pinto et al., 2017).

3 Results

3.1 Environmental conditions explored across sites

The experiments allowed us to explore a wide range of temperatures and photoperiod combinations. From all the locations, Salta site was cooler when compared to the rest of the sites (explored temperatures within the growing season were between 6 and 30 °C) due to its higher altitude above sea level. Capitán Miranda site offered the most inductive conditions for soybean development across sites, i.e. the highest average temperatures (10 to 39 °C) and shortest photoperiods during the growing season (11.1 to 13.9 h, Figure 2).

3.2 Genotypic and environmental variability in phenology

Due to the wide maturity group range of the evaluated soybean varieties (Table 2), site location (Table 1), and sowing dates from October to January across sites, a wide variation in days from sowing to developmental stages R1, R3, R5, R6, R7 and R8 (Fehr and Caviness, 1977) per genotype was observed (Figure 3). Variation in stages duration across genotypes and environments was reduced with advance of development, with coefficients of variation of 30.2, 25.1, 23.1, 20.7, 19.2, and 16.4% for stages R1, R3, R5, R6, R7, and R8, respectively. According to the phenological stage, this variation in the duration of the phases was mainly associated with the site and year (for all developmental stages). Sowing date and genotype affected all stages duration, with a smaller effects on R5-R6 and R7-R8 (Figure 4).

The EM-R1 phase was the one that showed the greatest variation in its duration and also was the one most affected by the MG and the genotype. Additionally, the genotypic variance given by both MG and genotype was decreasing with development, being the largest at the EM-R1 phase. Sowing date also produced larger variance early in the development, diminishing towards the end of the crop's cycle. The variance attributed to site was the largest at EM-R1 and R5-R6 phases, while the variance associated with the year was constant across developmental stages when considering absolute values but increasing in relative terms as development progressed, behaving in the same manner as the residual error (Figure 4).

3.3 Parameters linked to developmental responses to the environment

To derive a unique hierarchical model, two model selection stages were incorporated. At the first selection stage, which chose the best univariate model on a genotype basis, the best model in terms of out-of-sample predictive accuracy was model u4 (Table 5). Model u4 had three base temperatures that differed across developmental stages ($T_{\text{b}_{\text{SO-R1}}}, T_{\text{b}_{\text{R1-R5}}}, T_{\text{b}_{\text{R5-R7}}}$), and an extra parameter ΔP_{o} for calculating the photoperiod multiplier after R1 (Table 5).

Table 5: Univariate models tested by means of Pseudo-Bayesian model averaging (PBMA) and stacking (Yao et al., 2017). The higher the weight the better the model.

Model	Temperature response	Photoperiod response after R1	PBMA	Stacking
u1	$f(X_T, T_{\text{b}})$	$f(X_P, P_{\text{o}}, P_{\text{s}})$	0.035	0.0
u2		$f(X_P, P_{\text{o}}, P_{\text{s}}, \Delta P_{\text{o}})$	0.073	0.0
u3	$f(X_T, T_{\text{b}_{\text{SO-R1}}}, T_{\text{b}_{\text{R1-R5}}}, T_{\text{b}_{\text{R5-R7}}})$	$f(X_P, P_{\text{o}}, P_{\text{s}})$	0.273	0.0

Model	Temperature response	Photoperiod response after R1	PBMA	Stacking
u4		$f(X_P, P_\mathrm{o}, P_\mathrm{s}, \Delta P_\mathrm{o})$	0.619	1.0

At the second calibration stage, which tested whether parameters from model u4 were a function of maturity group, genotype, both or none, the best model was m4 (Table 6), whose full notation is

$$D_{\text{R0-R1}_{ij}} = (\beta_0^{D_{\text{R0-R1}}} + b_{0j}^{D_{\text{R0-R1}}}) + \beta_{\text{MG}}^{D_{\text{R0-R1}}} X_{\text{MG}_j} + \epsilon_{ij}^{D_{\text{R0-R1}}} \tag{24}$$

$$D_{\text{R1-R3}_{ij}} = (\beta_0^{D_{\text{R1-R3}}} + b_{0j}^{D_{\text{R1-R3}}}) + \beta_{\text{MG}}^{D_{\text{R1-R3}}} X_{\text{MG}_j} + \epsilon_{ij}^{D_{\text{R1-R3}}} \tag{25}$$

$$D_{\text{R3-R5}_{ij}} = (\beta_0^{D_{\text{R3-R5}}} + b_{0j}^{D_{\text{R3-R5}}}) + \beta_{\text{MG}}^{D_{\text{R3-R5}}} X_{\text{MG}_j} + \epsilon_{ij}^{D_{\text{R3-R5}}} \tag{26}$$

$$D_{\text{R5-R6}_{ij}} = (\beta_0^{D_{\text{R5-R6}}} + b_{0j}^{D_{\text{R5-R6}}}) + \epsilon_{ij}^{D_{\text{R5-R6}}} \tag{27}$$

$$D_{\text{R6-R7}_{ij}} = (\beta_0^{D_{\text{R6-R7}}} + b_{0j}^{D_{\text{R6-R7}}}) + \epsilon_{ij}^{D_{\text{R6-R7}}} \tag{28}$$

$$D_{\text{R7-R8}_{ij}} = (\beta_0^{D_{\text{R7-R8}}} + b_{0j}^{D_{\text{R7-R8}}}) + \epsilon_{ij}^{D_{\text{R7-R8}}} \tag{29}$$

$$T_{\text{b}_{\text{SO-R1}}ij} = \beta_0^{T_{\text{b}_{\text{SO-R1}}}} + \epsilon_{ij}^{T_{\text{b}_{\text{SO-R1}}}} \tag{30}$$

$$T_{\text{b}_{\text{R1-R5}}ij} = \beta_0^{T_{\text{b}_{\text{R1-R5}}}} + \epsilon_{ij}^{T_{\text{b}_{\text{R1-R5}}}} \tag{31}$$

$$T_{\text{b}_{\text{R5-R7}}ij} = \beta_0^{T_{\text{b}_{\text{R5-R7}}}} + \epsilon_{ij}^{T_{\text{b}_{\text{R5-R7}}}} \tag{32}$$

$$P_{\text{o}_{ij}} = (\beta_0^{P_\text{o}} + b_{0j}^{P_\text{o}}) + \beta_{\text{MG}}^{P_\text{o}} X_{\text{MG}_j} + \epsilon_{ij}^{P_\text{o}} \tag{33}$$

$$P_{\text{s}_{ij}} = (\beta_0^{P_\text{s}} + b_{0j}^{P_\text{s}}) + \epsilon_{ij}^{P_\text{s}} \tag{34}$$

$$\Delta P_{\text{o}_{ij}} = (\beta_0^{\Delta P_\text{o}} + b_{0j}^{\Delta P_\text{o}}) + \epsilon_{ij}^{\Delta P_\text{o}} \tag{35}$$

Parameters that concerned early plant development, i.e. vegetative and close to flowering stages, were the most affected by maturity group. Base temperatures did not change across maturity group or genotypes.

Table 6: Multivariate models differing in whether they included the terms $\beta_{\text{MG}} X_{\text{MG}_j}$ and b_{0j}, which respectively represent the linear response of the parameter to maturity group and the random intercept given by genotype. Their presence (1) or absence (0) is indicated separated by a slash, e.g. 1/1 indicates that the corresponding model included both $\beta_{\text{MG}} X_{\text{MG}_j}$ and b_{0j}. Models were compared by Pseudo-Bayesian model averaging (PBMA) and stacking (Yao et al., 2017). The higher the weight the better the model.

Model	$D_{\text{R0-R1}}$	$D_{\text{R1-R3}}$	$D_{\text{R3-R5}}$	$D_{\text{R5-R6}}$	$D_{\text{R6-R7}}$	$D_{\text{R7-R8}}$	$T_{\text{b}_{\text{SO-R1}}}$	$T_{\text{b}_{\text{R1-R5}}}$	$T_{\text{b}_{\text{R5-R7}}}$	P_o	P_s	ΔP_o	PBMA	Stacking
m1	1/1	1/1	1/1	1/1	1/1	1/1	1/1	1/1	1/1	1/1	1/1	1/1	0.056	0.087
m2	1/1	1/1	1/1	1/1	0/1	0/1	0/1	0/1	0/1	1/1	0/1	0/1	0.203	0.188
m3	1/1	1/1	1/1	1/1	0/1	0/1	0/0	0/0	0/0	1/1	0/1	0/1	0.159	0.009
m4	1/1	1/1	1/1	0/1	0/1	0/1	0/0	0/0	0/0	1/1	0/1	0/1	0.266	0.280
m5	1/1	1/1	0/1	0/1	0/1	0/1	0/0	0/0	0/0	1/1	0/1	0/1	0.196	0.147
m6	1/1	1/1	1/1	1/1	0/1	0/0	0/0	0/0	0/0	1/1	0/1	0/0	0.001	0.062
m7	1/1	1/1	1/1	1/1	0/1	0/0	0/0	0/0	0/0	1/1	0/1	0/1	0.023	0.080
m8	1/1	1/1	1/0	1/1	0/1	0/1	0/0	0/0	0/0	1/1	0/1	0/1	0.096	0.146
m9	1/1	1/1	1/1	1/1	0/0	0/1	0/0	0/0	0/0	1/1	0/1	0/1	0.000	0.000

3.4 Developmental drivers of soybean maturity groups

Optimum photoperiod P_o, and photothermal days $D_{\text{R0-R1}}$, $D_{\text{R1-R3}}$ and $D_{\text{R3-R5}}$, were linearly related to MG (Figure 5, a). Photothermal days $D_{\text{R5-R6}}$, $D_{\text{R6-R7}}$, calendar days $D_{\text{R7-R8}}$, photoperiod sensitivity P_s and the reduction in critical

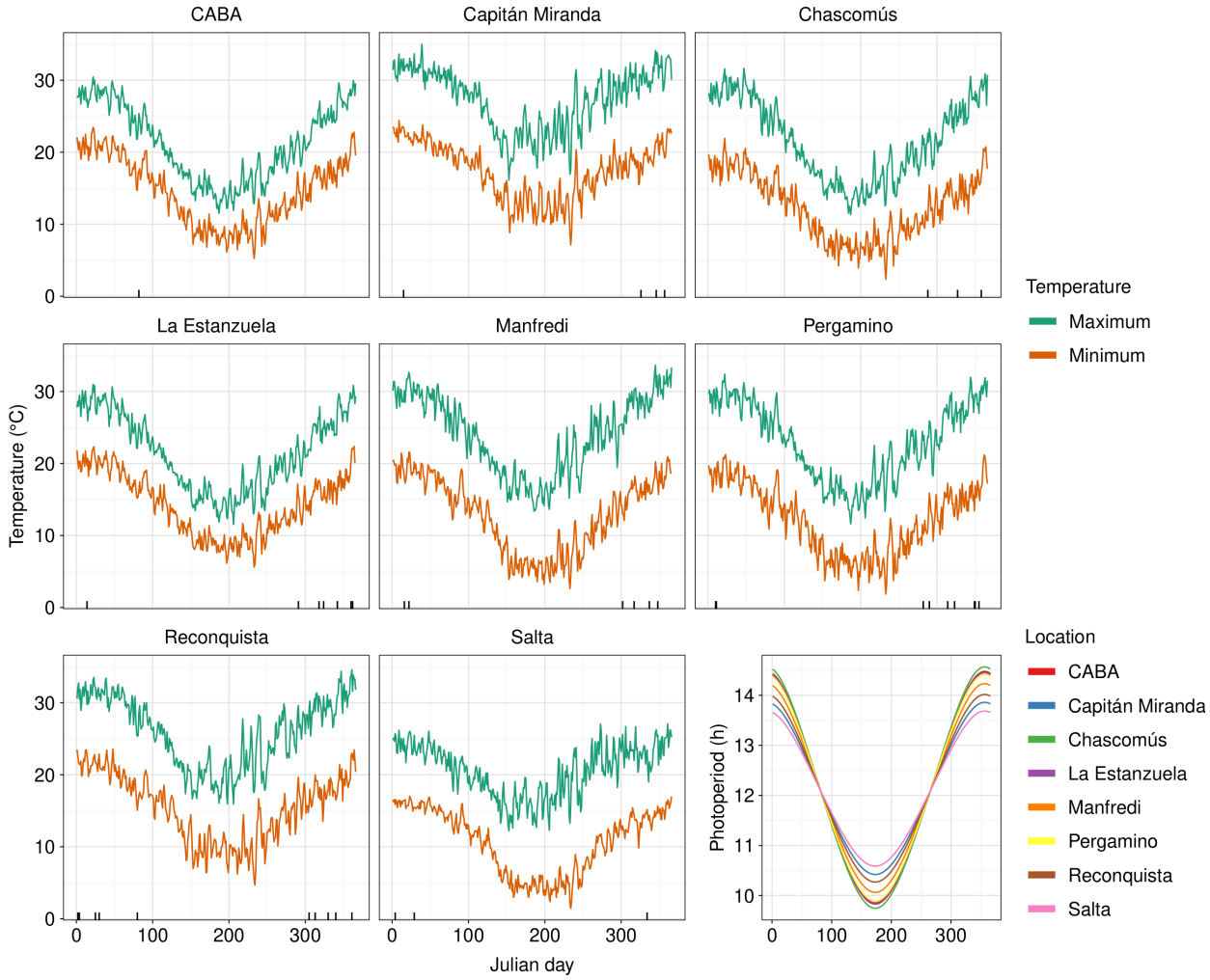

Figure 2: Average minimum and maximum daily temperatures for each experimental site during the evaluated years, and daily photoperiod for each location. Short, vertical segments along the x axis show the sowing dates at each location. The last sub-figure shows a summary of the photoperiod dynamics for all locations.

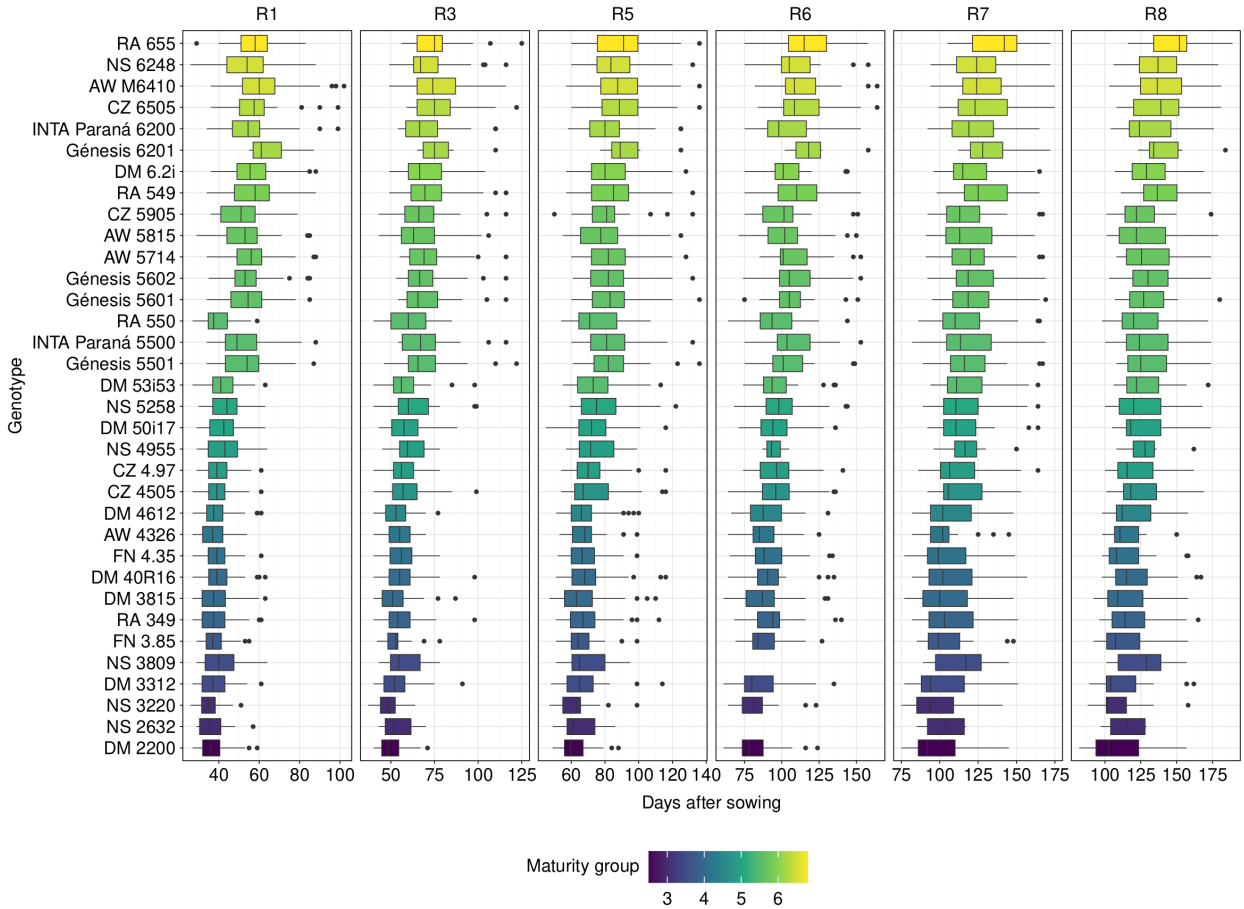

Figure 3: Variability in the developmental stages expressed as days from sowing to stages R1, R3, R5, R6, R7 and R8 (Fehr and Caviness, 1977). Each boxplot shows the data range explored across the sowing dates and locations as listed in Table 1.

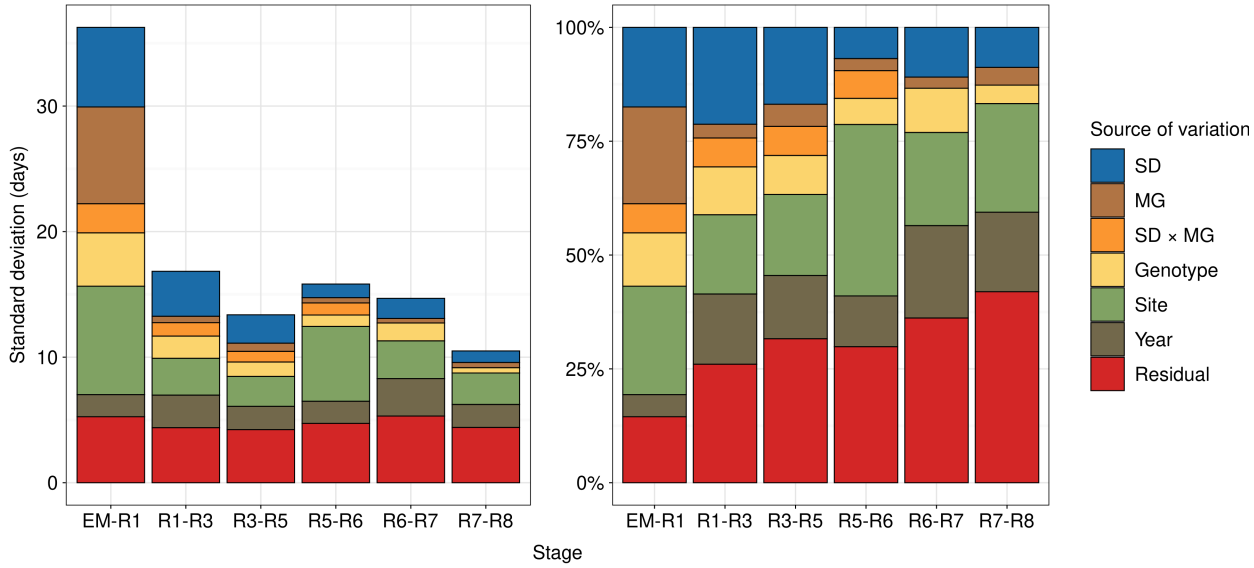

Figure 4: Standard deviation in stages duration partitioned per source of variation, represented as absolute (days, left) or relative (%, right) duration. Colours represent the different sources of variance such as sowing date (SD), maturity group (MG), and their interaction (SD × MG).

photoperiod threshold after R1, ΔP_o, were unrelated to MG but differed between genotypes (Figure 5, b). Base temperatures $T_{b_{SO\text{-}R1}}$, $T_{b_{R1\text{-}R5}}$ and $T_{b_{R5\text{-}R7}}$ were constant across genotypes and therefore can be considered species-specific (Figure 5, c). Optimum photoperiod P_o was the parameter most closely related to MG (Figure 5, a). Despite $T_{b_{SO\text{-}R1}}$ (0.054 °C, CI: -0.03 to 0.14 °C) was slightly higher than $T_{b_{R1\text{-}R5}}$ (-0.07 °C, CI: -0.15 to 0.013 °C, probability of direction [PD] = 96%), this difference was almost negligible when calculating the temperature multiplier ϕ_T for stages SO-R1 and R5-R7 (Figure 5, d). Base temperature for grain filling ($T_{b_{R5\text{-}R7}}$) was negative (-19.2 °C, CI: -19.8 to -18.5 °C), much lower than vegetative ($T_{b_{SO\text{-}R1}}$) and post-flowering ($T_{b_{R1\text{-}R5}}$) base temperatures (Figure 5, c). This is in spite soybean does not survive freezing temperatures. However, this negative base temperature enhanced the predictive ability of our model, similarly to the findings of Boote et al. (1998b). The photoperiod multiplier ϕ_P as a function of photoperiod (Figure 5, e) showed a marked difference in P_o between contrasting genotypes DM 2200 (MG 2, 13.0 h, CI: 12.9 to 13.0 h) and RA 550 (MG 5.5, 12.4 h, CI: 12.4 to 12.5 h), but the slopes in the photoperiod response region were not visually evident in spite their differences in P_s (0.292 h^{-1}, CI: 0.289 to 0.295 h^{-1} vs 0.296 h^{-1}, CI: 0.293 to 0.299 h^{-1}, PD = 92%)

3.5 Model's ability to predict phenology

To assess the phenological accuracy of the calibrated model, each genotype's prediction was validated against the validation data set. The model accurately predicted soybean phenology with an increased prediction error at later phenological stages (Table 7). The average RMSE for stages R1, R3, R5, R6, R7 and R8 was 5.8, 7.1, 7.4, 9.4, 8.5, and 9.5 days, respectively, representing 12.1, 11.0, 9.4, 9.3, 7.3, 7.5% in terms of the mean observed days after sowing (DAS) of each stage (Table 7). From those errors, the RLA, measuring the percentage of error given by a systematic deviation from the 1:1 line, was 43.1, 5.3, 15.1, 8.8, 17.2, and 17.2% for stages R1, R3, R5, R6, R7 and R8, respectively (Table 7), showing that this deviation was much higher for R1 than the rest of the stages. On a location basis, the RMSE was highest for Manfredi (Table 7), but these errors were less biased than those of Salta (17.2 vs 83.2% in RLA; Figure 6 and Figure 7). Salta showed biased errors towards the end of the reproductive stage (R6, R7 and R8, Table 7, Figure 6 and Figure 7). Overall, the model showed a very good level of prediction with RMSE values from 5.8 to 9.5 days and RRMSE from 12.1 to 7.5% for R1 to R8 developmental stages.

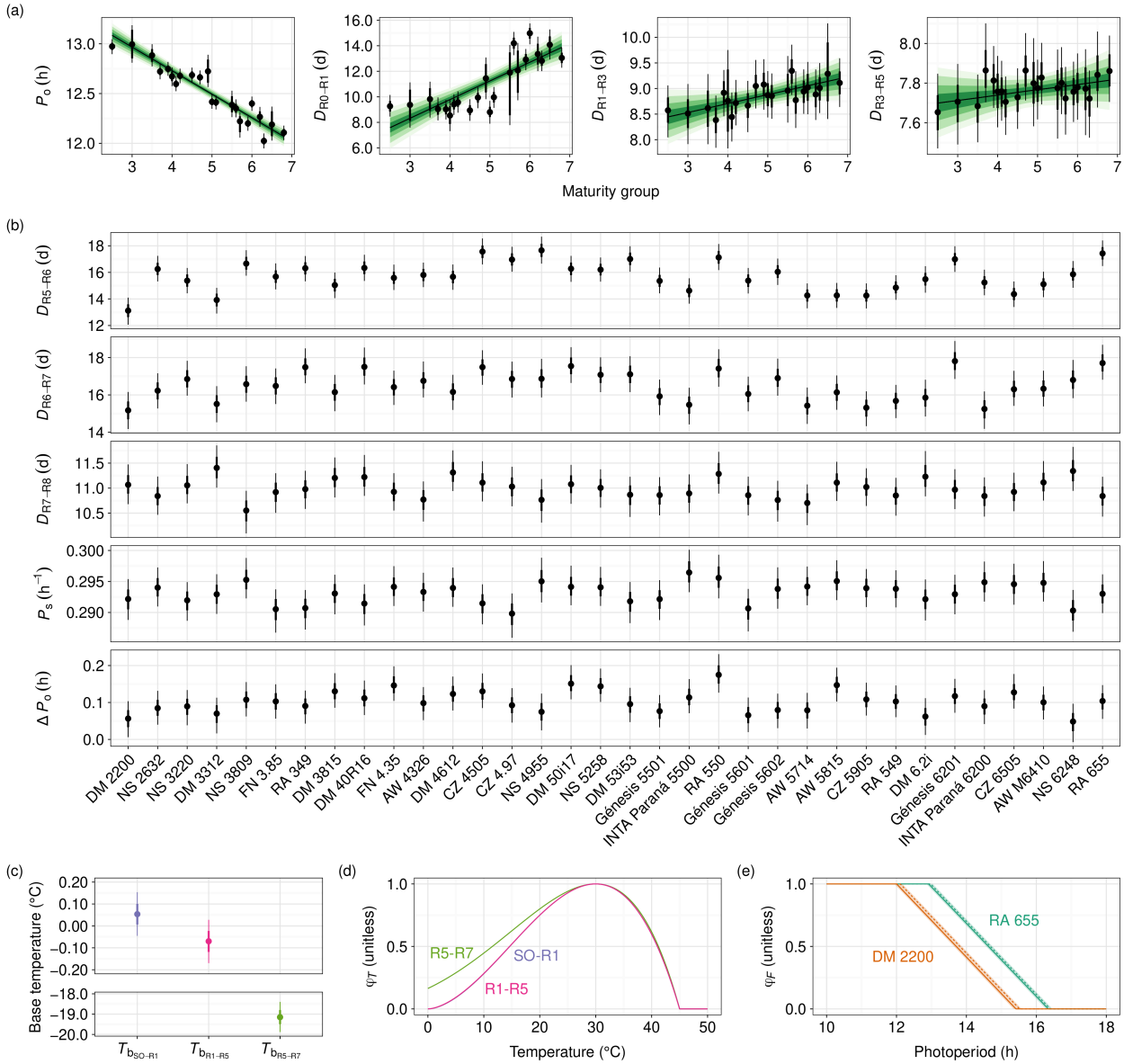

Figure 5: Parameters of model u4 (Table 5) as modelled by the multivariate model m4 (Table 6). (a) Parameters P_o, $D_{R0\text{-}R1}$, $D_{R1\text{-}R3}$ and $D_{R3\text{-}R5}$ as a function of maturity group, where the solid line represents the median regression line and green shades depict credible intervals 50, 90, 95 and 99%. (b) Parameters that showed no relationship with maturity group but a random effect (random intercept) of genotype instead. (c) Genotype-independent base temperatures $T_{b_{SO\text{-}R1}}$, $T_{b_{R1\text{-}R5}}$ and $T_{b_{R5\text{-}R7}}$. (d) Temperature multiplier ϕ_T as a function of temperature for stages sowing-R1 (SO-R1) R1-R5 and R5-R7. Notice that curves for SO-R1 and R1-R5 overlap each other almost entirely and thus cannot be visually distinguished (despite their different base temperatures). (e) Photoperiod multiplier ϕ_P as a function of photoperiod for the most contrasting genotypes in terms of P_o, P_s and ΔP_o (DM 2200 [MG 2] and RA 550 [MG 5.5]), and for stages before (solid line) and after R1 (dashed line). From (a) to (e), points show the median fitted value and bars represent the 50 (thicker) and 90% (thinner) credible intervals.

Table 7: The ability of the multivariate model to predict developmental stages across all genotypes. Root mean squared errors (RMSE, days), relative root mean squared errors (RRMSE, %), and relative lack of accuracy (RLA, %) for all tested locations as well as across them (total) for stages R1, R3, R5, R6, R7 and R8.

		Stage						
	Metric	R1	R3	R5	R6	R7	R8	Total
Capitán Miranda	RMSE (d)	3.5	4.9	3.9	5.6	5.5	6.4	5.1
	RRMSE (%)	9.1	8.7	6.0	6.5	5.5	5.9	6.7
	RLA (%)	18.2	55.9	26.6	44.7	42.3	50.5	11.6
Chascomús	RMSE (d)	7.3	4.1	6.3	—	3.5	4.6	5.9
	RRMSE (%)	11.4	5.4	7.2	—	2.5	2.9	7.2
	RLA (%)	74.6	39.1	58.1	—	100.0	100.0	2.1
La Estanzuela	RMSE (d)	6.0	6.4	5.6	10.4	6.2	8.8	7.5
	RRMSE (%)	10.8	9.4	6.8	9.4	5.0	6.6	7.8
	RLA (%)	39.8	10.5	1.3	54.2	34.0	32.6	2.1
Manfredi	RMSE (d)	7.1	10.7	10.6	15.6	11.4	11.2	11.3
	RRMSE (%)	14.9	15.9	13.0	14.2	9.1	8.3	12.3
	RLA (%)	30.3	22.8	30.7	43.6	9.5	3.5	17.1
Pergamino	RMSE (d)	7.5	7.8	8.6	7.3	6.5	9.0	7.8
	RRMSE (%)	13.7	10.9	9.5	6.7	5.2	7.0	8.3
	RLA (%)	59.2	42.1	54.9	15.8	53.8	46.9	2.2
Reconquista	RMSE (d)	4.1	4.2	6.3	3.9	10.0	8.4	6.1
	RRMSE (%)	10.7	7.6	9.2	4.6	9.7	6.9	8.7
	RLA (%)	36.8	30.8	72.0	22.3	17.1	11.3	0.8
Salta	RMSE (d)	2.0	6.5	5.5	11.6	18.6	19.6	9.8
	RRMSE (%)	4.5	11.8	8.0	12.4	16.8	16.1	14.0
	RLA (%)	4.7	81.4	88.2	84.9	96.0	96.2	82.4
Total	RMSE (d)	5.8	7.1	7.4	9.4	8.6	9.6	7.9
	RRMSE (%)	12.0	11.1	9.4	9.3	7.3	7.6	9.3
	RLA (%)	42.8	5.3	15.1	9.2	17.0	17.3	0.7

3.6 Model predictions for website deployment

The algorithms generated to predict each of the developmental stages of the soybean crop were included in a software named CRONOSOJA (http://cronosoja.agro.uba.ar/). The software is simple and friendly for the users, who can select a location within the country (Argentina, Paraguay or Uruguay), a genotype, and a particular sowing date. The model returns predicted dates of the different phenological stages with an estimated error value. In addition, the CRONOSOJA model indicates the critical period of the crop, the risk of frost for each of the phenological stages and the dynamics of plant available water in the profile (Figure 8).

4 Discussion

Field experiments in different countries (Argentina, Uruguay and Paraguay) were conducted to evaluate phenology in soybean varieties, grown over a range of latitudes from -24.9 to -35.6, and at different sowing dates between October and January, allowing us to explore a wide range of thermo-photoperiodic conditions. The combination of a wide range of environmental conditions and MG from 2 to 6 allowed us to precisely dissect soybean developmental

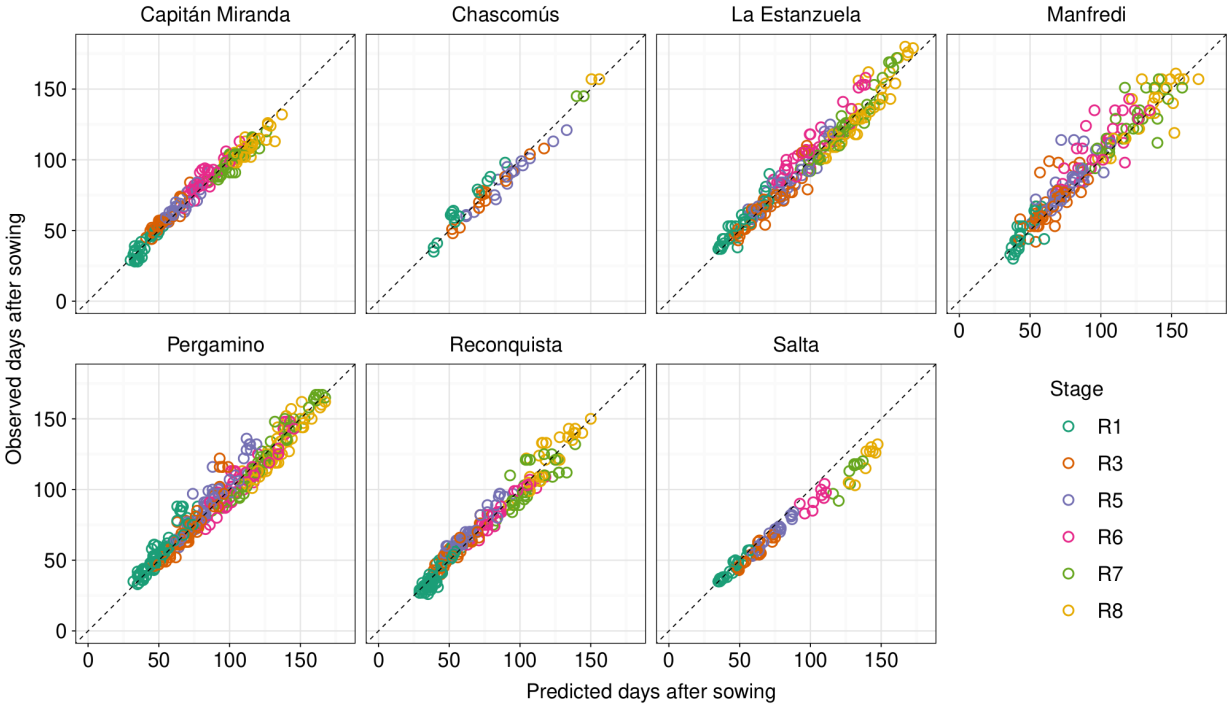

Figure 6: Observed days after sowing as a function of predicted days after sowing for stages R1, R3, R5, R6, R7 and R8 evaluated with data from the validation data sets at all sites using the multivariate model. The dashed line represents the $y = x$ line.

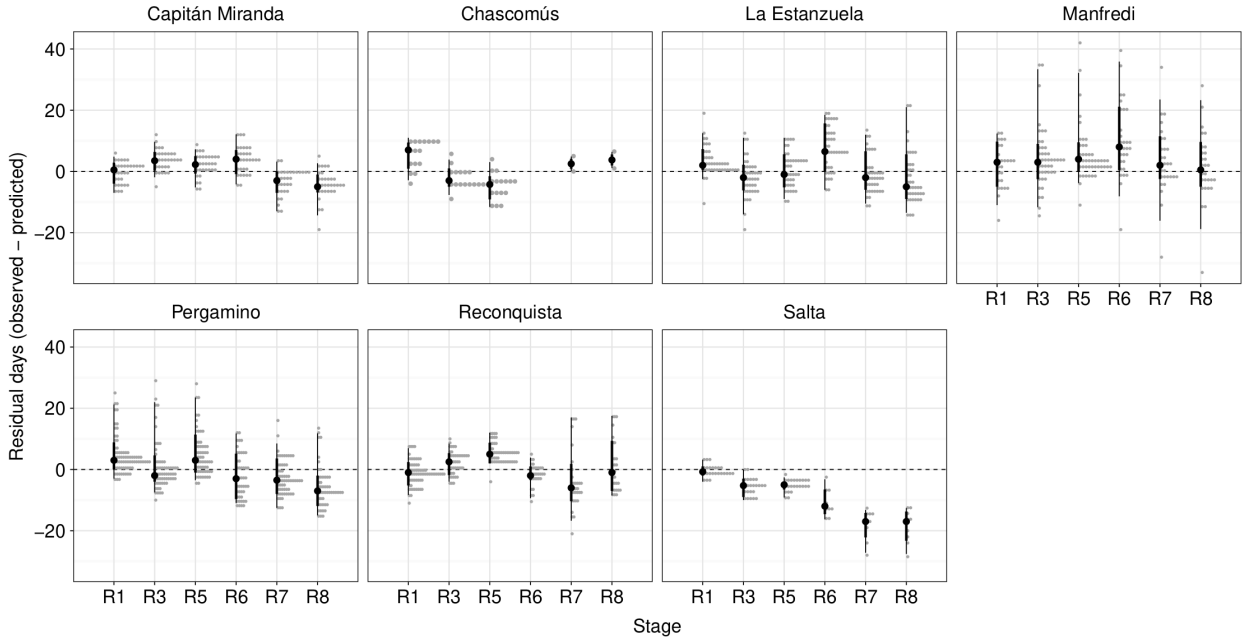

Figure 7: Evaluation of the difference between observed and predicted days after sowing for stages R1, R3, R5, R6, R7 and R8 at all sites using the validation data set. Black points represent the median, whereas the thick and thinner lines show the 50 and 90% credible intervals. Grey dots show the distribution of the residuals as counts

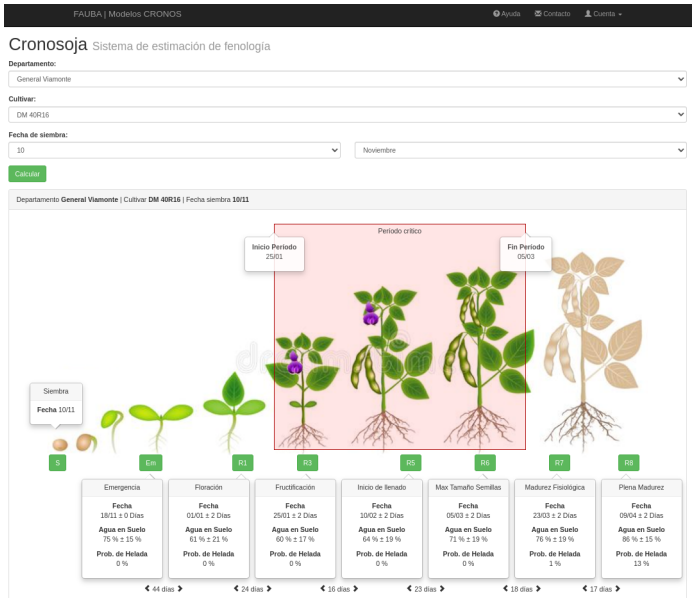

Figure 8: Example of the output information from the CRONOSOJA model in the web version where the prediction dates of the model for the different phenological stages are detailed. The red shaded rectangle indicates the time interval of occurrence of the critical period.

responses to the environment. In this context, three base temperatures that differed across developmental stages and an extra parameter for calculating the photoperiod multiplier after R1 were identified, in line with previous studies (Boote et al., 2003; Grimm et al., 1994; Grimm et al., 1993; Piper et al., 1996). A wide range of variation in the length of the phases from sowing to different developmental stages across different genotypes was explored to select between alternative phenological models that best explained the observed experimental data.

A rapid method of model selection by means of best predictive accuracy was employed (Vehtari et al., 2017) in a dynamic developmental model (Jones et al., 2003; Keating et al., 2003). This allowed us to rapidly assess which model structure was the best. An alternative would be to perform another type of cross-validation called k-fold, as used previously by Wallach et al. (2001), but this would have been unfeasible in our case as it would have taken much more computational time given the large number of iterations required to reach convergence of the Bayesian model. Using our framework as a proxy for model parsimony, we were able to choose meaningful structures for our models, whereby our understanding of the processes determining phenology was increased. For instance, we were able to corroborate in field conditions that soybean's sensitivity to photoperiod increased after flowering (Table 5). The parameter representing this extra sensitivity, ΔP_{o}, is already included in DSSAT-CROPGRO as a parameter called R1PPO (Boote et al., 1998a) but is absent in APSIM Soybean (Robertson et al., 2002). Regarding base temperature, some models suggest a constant value for predicting soybean phenology. Cober et al. (2001) proposed a constant base temperature of 5.8 °C to predict flowering time. Similarly, Hadley et al. (1984) and Major et al. (1975a) showed that base temperature to predict flowering time, when photoperiods were longer than the optimum value, was 7.8 °C without differences among the used varieties. However, a model with variable base temperatures, during vegetative, reproductive and grain filling phases, was better than a model considering constant base temperatures (Table 5). Moreover, we found lower base temperatures compared to those authors, although this may obey to our choice of a curvilinear function instead of a linear one to explain temperature effects (Equation 2, Equation 3, Figure 5, d). Variable base temperatures are already formalised in DSSAT-CROPGRO (Boote et al., 1998b; Grimm et al., 1993) but not in APSIM Soybean, which uses a constant base temperature (Robertson et al., 2002). The present work suggests that the latter modelling platform could benefit from including ΔP_{o} and a stage-dependent T_{b} to its inner functions.

Model selection also showed that changes in the determinants of phenology across maturity groups were mainly due to processes occurring early in reproductive development, around phases EM-R1, R1-R3 and R3-R5 (Figure 5, a). Moreover, the differences between cultivars were due to photoperiod sensitivity, with similar responses to tem-

perature (Grimm et al., 1993). In contrast to Piper et al. (1996), who showed no association between parameters controlling the duration of R1-R5 phases, we discovered that photothermal days for these stages were a linear function of maturity group. However, P_o, the optimum photoperiod affecting all developmental stages between the end of the juvenile phase and physiological maturity, was the parameter that best correlated with the maturity group. This finding suggests that P_o may be a good proxy to estimate maturity groups when there are ambiguities in their determination by seed companies. We did not detect a relationship between maturity group and photoperiod sensitivity, P_s, as reported by Piper et al. (1996) and as it is parameterised in DSSAT-CROPGRO model (Boote et al., 2003). This may be due to a weakness of model fitting given the high of collinearity between P_o and P_s, in spite our attempt to improve this issue by imposing mild informative priors over them (Table 4).

The ability of the model to predict phenology was greater for early stages of development (Table 7). Predictions for later stages were less accurate, in accordance with Salmerón and Purcell (2016). This is in agreement with our pre-modelling quantification of sources of variation for stages duration, which showed that the fraction of unexplained variance increased towards the end of the developmental cycle (Figure 4). The model underpredicted development rate in cool environments like Salta, an issue already reported by Piper et al. (1996) that may highlight a weakness of the model to represent soybean development at low temperatures.

The outputs of the selected model that works at the level of genotypes or maturity group were included within a user-friendly interphase called CRONOSOJA (http://cronosoja.agro.uba.ar/), which is available for free and includes all soybean productive regions from Argentina, Paraguay and Uruguay.

5 Conclusions

The results of the study showed that parameters concerning early plant development, such as those affecting stages of vegetative growth and flowering, were the most affected by the different maturity groups (MG). However, base temperatures did not change across MG or between genotypes. The optimum photoperiod P_o, and photothermal days $D_{\text{R0-R1}}$, $D_{\text{R1-R3}}$ and $D_{\text{R3-R5}}$, were linearly related to MG. Photothermal days $D_{\text{R5-R6}}$, $D_{\text{R6-R7}}$, calendar days $D_{\text{R7-R8}}$, photoperiod sensitivity P_s and the reduction in optimum photoperiod threshold after R1, ΔP_o, were unrelated to MG but differed among genotypes. Base temperatures $T_{b_{\text{SO-R1}}}$, $T_{b_{\text{R1-R5}}}$ and $T_{b_{\text{R5-R7}}}$, were constant across genotypes and can be considered species-specific. The optimum photoperiod P_o was the parameter most closely related to MG.

6 Funding

This work was funded by project “Bases fisiológicas y genéticas de las respuestas de trigo y soja a limitantes bióticas y abióticas: estudios orientados al mejoramiento genético y al manejo de los cultivos en el Cono Sur” from PROCISUR.

7 Acknowledgements

We thank Francisco Raspa, Luis Blanco, and Octavio Ghio Trebino for their dedication and hard work in conducting the field experiments, which greatly enhanced the quality and impact of this scientific article.

8 References

Aitken, Y., 1974. Flowering time, climate and genotype: The adaptation of agricultural species to climate through flowering responses. Melbourne University Press, Carlton, Vic.

Archontoulis, S.V., Miguez, F.E., Moore, K.J., 2014. A methodology and an optimization tool to calibrate phenology of short-day species included in the APSIM PLANT model: Application to soybean. Environmental Modelling & Software 62, 465–477. https://doi.org/10.1016/j.envsoft.2014.04.009

Bates, D., Mächler, M., Bolker, B., Walker, S., 2015. Fitting linear mixed-effects models using lme4. Journal of Statistical Software 67, 1–48. https://doi.org/10.18637/jss.v067.i01

Boote, K.J., Jones, J.W., Batchelor, W.D., Nafziger, E.D., Myers, O., 2003. Genetic coefficients in the CROPGRO–soybean model. Agronomy Journal 95, 32–51.

Boote, K.J., Jones, J.W., Hoogenboom, Gerrit, 1998a. Simulation of crop growth: CROPGRO model, in: Peart, R.M., Curry, R.B. (Eds.), Agricultural Systems Modeling and Simulation. CRC Press.

Boote, K.J., Jones, J.W., Hoogenboom, G., Pickering, N.B., 1998b. The CROPGRO model for grain legumes, in: Tsuji, G.Y., Hoogenboom, G., Thornton, P.K. (Eds.), Understanding Options for Agricultural Production, Systems Approaches for Sustainable Agricultural Development. Springer Netherlands, Dordrecht, pp. 99–128. https://doi.org/10.1007/978-94-017-3624-4_6

Bürkner, P.-C., 2018. Advanced bayesian multilevel modeling with the R package brms. The R Journal 10, 395. https://doi.org/10.32614/RJ-2018-017

Calviño, P.A., Sadras, V.O., Andrade, F.H., 2003. Quantification of environmental and management effects on the yield of late-sown soybean. Field crops research 83, 67–77.

Carpenter, B., Gelman, A., Hoffman, M.D., Lee, D., Goodrich, B., Betancourt, M., Brubaker, M., Guo, J., Li, P., Riddell, A., 2017. Stan: A probabilistic programming language. Journal of Statistical Software 76. https://doi.org/10.18637/jss.v076.i01

Cober, E.R., Stewart, D.W., Voldeng, H.D., 2001. Photoperiod and temperature responses in early-maturing, near-isogenic soybean lines. Crop Science 41, 721–727. https://doi.org/10.2135/cropsci2001.413721x

Correndo, A.A., Hefley, T.J., Holzworth, D.P., Ciampitti, I.A., 2021. Revisiting linear regression to test agreement in continuous predicted-observed datasets. Agricultural Systems 192, 103194. https://doi.org/10.1016/j.agsy.2021.103194

Dunphy, E.J., Hanway, J.J., Green, D.E., 1979. Soybean yields in relation to days between specific developmental stages1. Agronomy Journal 71, 917–920. https://doi.org/10.2134/agronj1979.00021962007100060005x

Eddelbuettel, D., François, R., 2011. Rcpp: Seamless R and C++ integration. Journal of Statistical Software 40. https://doi.org/10.18637/jss.v040.i08

Egli, D.B., 1998. Seed biology and the yield of grain crops. CAB international.

Egli, D.B., Bruening, W.P., 2000. Potential of early-maturing soybean cultivars in late plantings. Agronomy Journal 92, 532–537. https://doi.org/10.2134/agronj2000.923532x

Fehr, W.R., Caviness, C.E., 1977. Stages of soybean development.

Fernández-Long, M.E., Natalia, G., Spennemann, P., 2018. Inter-comparación y validación de simulaciones de la humedad del suelo en la Pampa Húmeda.

Fernández-Long, M.E., Peretti, M., Carnelos, D., Della-Chiesa, T., Spescha, L., 2021. Characterization of the seasonal variation of soil moisture in Argentina. International Journal of Climatology 41. https://doi.org/10.1002/joc.6705

Fernández-Long, M.E., Spescha, L., Barnatán, I., Murphy, G., 2013. Modelo de balance hidrológico operativo para el agro (BHOA). Agronomía & Ambiente 32.

Garibaldi, L.A., Aristimuño, F.J., Oddi, F.J., Tiribelli, F., 2017. Inferencia multimodelo en ciencias sociales y ambientales. Ecología Austral 27, 348–363.

Garner, W.W., Allard, H.A., 1930. Photoperiodic response of soybeans in relation to temperature and other environmental factors. Journal of Agricultural Research 41.

Grimm, S.S., Jones, J.W., Boote, K.J., Herzog, D.C., Herzog, D.C., 1994. Modeling the occurrence of reproductive stages after flowering for four soybean cultivars. Agronomy Journal 86, 31–38. https://doi.org/10.2134/agronj1994.00021962008600010007x

Grimm, S.S., Jones, J.W., Boote, K.J., Hesketh, J.D., 1993. Parameter estimation for predicting flowering date of soybean cultivars. Crop Science 33, 137–144. https://doi.org/10.2135/cropsci1993.0011183X003300010025x

Hadley, P., Roberts, E.H., Summerfield, R.J., Minchin, F.R., 1984. Effects of temperature and photoperiod on flowering in soya bean [Glycine max (L.) Merrill]: A quantitative model. Annals of Botany 53, 669–681.

Hartig, F., Minunno, F., Paul, S., 2019. BayesianTools: General-purpose MCMC and SMC samplers and tools for bayesian statistics.

Hersbach, H., Bell, B., Berrisford, P., Biavati, G., Horányi, A., Muñoz Sabater, J., Nicolas, J., Peubey, C., Radu, R., Rozum, I., Schepers, D., Simmons, A., Soci, C., Dee, D., Thépaut, J.-N., 2018. ERA5 hourly data on single levels from 1979 to present. Copernicus climate change service (C3S) climate data store (CDS).

Hijmans, R.J., 2021. Geosphere: Spherical trigonometry.

Jiang, H., Egli, D.B., 1995. Soybean seed number and crop growth rate during flowering. Agronomy Journal 87, 264–267. https://doi.org/10.2134/agronj1995.00021962008700020020x

Jones, C.A., Ritchie, J.T., Kiniry, J.R., Godwin, D.C., 1986. Subroutine structure, in: Jones, C.A., Kiniry, J.R., Dyke, P.T. (Eds.), CERES-Maize: A Simulation Model of Maize Growth and Development. Texas A&M University Press, College Station, pp. 49–111.

Jones, J.W., Hoogenboom, G., Porter, C.H., Boote, K.J., Batchelor, W.D., Hunt, L.A., Wilkens, P.W., Singh, U., Gijsman, A.J., Ritchie, J.T., 2003. The DSSAT cropping system model. European Journal of Agronomy, Modelling Cropping Systems: Science, Software and Applications 18, 235–265. https://doi.org/10.1016/S1161-0301(02)00107-7

Kantolic, A.G., Peralta, G.E., Slafer, G.A., 2013. Seed number responses to extended photoperiod and shading during reproductive stages in indeterminate soybean. European Journal of Agronomy 51, 91–100. https://doi.org/10.1016/j.eja.2013.07.006

Kantolic, A.G., Slafer, G.A., 2007. Development and seed number in indeterminate soybean as affected by timing and duration of exposure to long photoperiods after flowering. Annals of Botany 99, 925–933. https://doi.org/10.1093/aob/mcm033

Kantolic, A.G., Slafer, G.A., 2001. Photoperiod sensitivity after flowering and seed number determination in indeterminate soybean cultivars. Field Crops Research 72, 109–118. https://doi.org/10.1016/S0378-4290(01)00168-X

Keating, B.A., Carberry, P.S., Hammer, G.L., Probert, M.E., Robertson, M.J., Holzworth, D., Huth, N.I., Hargreaves, J.N., Meinke, H., Hochman, Z., 2003. An overview of APSIM, a model designed for farming systems simulation. European Journal of Agronomy 18, 267–288.

Lawn, R.J., Summerfield, R.J., Ellis, R.H., Qi, A., Roberts, E.H., Chay, P.M., Brouwer, J.B., Rose, J.L., Yeates, S.J., 1995. Towards the reliable prediction of time to flowering in six annual crops. VI. Applications in crop improvement. Experimental Agriculture 31, 89–108. https://doi.org/10.1017/S0014479700025047

Lüdecke, D., Waggoner, P., Makowski, D., 2019. Insight: A unified interface to access information from model objects in R. Journal of Open Source Software 4, 1412. https://doi.org/10.21105/joss.01412

Major, D.J., Johnson, D.R., Luedders, V.D., 1975a. Evaluation of eleven thermal unit methods for predicting soybean development 1. Crop Science 15, 172–174.

Major, D.J., Johnson, D.R., Tanner, J.W., Anderson, I.C., 1975b. Effects of daylength and temperature on soybean development. Crop Science 15, 174–179. https://doi.org/10.2135/cropsci1975.0011183x001500020009x

Mayers, J., Lawn, R., Byth, D., 1991. Adaptation of soybean (glycine max (L.) merrill) to the dry season of the tropics. I. Genotypic and environmental effects on phenology. Australian Journal of Agricultural Research 42, 497. https://doi.org/10.1071/AR9910497

Miralles, D.J., Slafer, G.A., 1999. Wheat development, in: Satorre, E.H., Slafer, G.A. (Eds.), Wheat: Ecology and Physiology of Yield Determination. Food Products Press, New York.

Monzon, J.P., Cafaro La Menza, N., Cerrudo, A., Canepa, M., Rattalino Edreira, J.I., Specht, J., Andrade, F.H., Grassini, P., 2021. Critical period for seed number determination in soybean as determined by crop growth rate, duration, and dry matter accumulation. Field Crops Research 261, 108016. https://doi.org/10.1016/j.fcr.2020.108016

Nico, M., Miralles, D.J., Kantolic, A.G., 2019. Natural post-flowering photoperiod and photoperiod sensitivity: Roles in yield-determining processes in soybean. Field Crops Research 231, 141–152. https://doi.org/10.1016/j.fcr.2018.10.019

Nico, M., Miralles, D.J., Kantolic, A.G., 2015. Post-flowering photoperiod and radiation interaction in soybean yield determination: Direct and indirect photoperiodic effects. Field Crops Research 176, 45–55. https://doi.org/10.1016/j.fcr.2015.02.018

Pebesma, E., 2018. Simple features for R: Standardized support for spatial vector data. The R Journal 10, 439–446. https://doi.org/10.32614/RJ-2018-009

Penalba, O.C., Pántano, V.C., Spescha, L.B., Murphy, G.M., 2019. El Niño-Southern Oscillation incidence over long dry sequences and their impact on soil water storage in Argentina. International Journal of Climatology 39, 2362–2374. https://doi.org/10.1002/joc.5957

Peretti, M., Spennemann, P.C., Fernández-Long, M.E., 2023. Trends in soil moisture content and water deficits in Argentina and the role of climate contribution. Theoretical and Applied Climatology 152, 1189–1201. https://doi.org/10.1007/s00704-023-04428-x

Pinto, P., Fernández-Long, M.E., Piñeiro, G., 2017. Including cover crops during fallow periods for increasing ecosystem services: Is it possible in croplands of Southern South America? Agriculture, Ecosystems & Environment 248, 48–57. https://doi.org/10.1016/j.agee.2017.07.028

Piper, E.L., Boote, K.J., Jones, J.W., Grimm, S.S., 1996. Comparison of two phenology models for predicting flowering and maturity date of soybean. Crop Science 36, 1606–1614.

Plummer, M., Best, N., Cowles, K., Vines, K., 2006. CODA: Convergence diagnosis and output analysis for MCMC. R News 6, 7–11.

R Core Team, 2022. R: A language and environment for statistical computing. R Foundation for Statistical Computing, Vienna, Austria.

Robertson, M.J., Carberry, P.S., Huth, N.I., Turpin, J.E., Probert, M.E., Poulton, P.L., Bell, M., Wright, G.C., Yeates, S.J., Brinsmead, R.B., 2002. Simulation of growth and development of diverse legume species in APSIM. Australian Journal of Agricultural Research 53, 429–446. https://doi.org/10.1071/ar01106

Salmerón, M., Purcell, L.C., 2016. Simplifying the prediction of phenology with the DSSAT-CROPGRO-soybean model based on relative maturity group and determinacy. Agricultural Systems 148, 178–187. https://doi.org/10.1016/j.agsy.2016.07.016

Schulzweida, U., 2021. CDO user guide. https://doi.org/10.5281/zenodo.5614769

Setiyono, T.D., Weiss, A., Specht, J., Bastidas, A.M., Cassman, K.G., Dobermann, A., 2007. Understanding and modeling the effect of temperature and daylength on soybean phenology under high-yield conditions. Field Crops Research 100, 257–271. https://doi.org/10.1016/j.fcr.2006.07.011

Severini, A.D., Wasson, A.P., Evans, J.R., Richards, R.A., Watt, M., 2020. Root phenotypes at maturity in diverse wheat and triticale genotypes grown in three field experiments: Relationships to shoot selection, biomass, grain yield, flowering time, and environment. Field Crops Research 255, 107870. https://doi.org/10.1016/j.fcr.2020.107870

Silge, J., Chow, F., Kuhn, M., Wickham, H., 2021. Rsample: General resampling infrastructure.

Slafer, G.A., Rawson, H.M., 1994. Sensitivity of wheat phasic development to major environmental factors: A reexamination of some assumptions made by physiologists and modellers. Functional Plant Biology 21, 393–426. https://doi.org/10.1071/pp9940393

Spennemann, P.C., Fernández-Long, M.E., Gattinoni, N.N., Cammalleri, C., Naumann, G., 2020. Soil moisture evaluation over the Argentine Pampas using models, satellite estimations and in-situ measurements. Journal of Hydrology: Regional Studies 31, 100723. https://doi.org/10.1016/j.ejrh.2020.100723

Stoffel, M.A., Nakagawa, S., Schielzeth, H., 2020. partR2: Partitioning R^2 in generalized linear mixed models (preprint). Bioinformatics. https://doi.org/10.1101/2020.07.26.221168

Summerfield, R., 1998. Characterization of the photoperiodic response of post-flowering development in maturity isolines of soyabean [glycine max (L.) merrill] 'clark'. Annals of Botany 82, 765–771. https://doi.org/10.1006/anbo.1998.0755

Vehtari, A., Gabry, J., Yao, Y., Gelman, A., 2019. Loo: Efficient leave-one-out cross-validation and WAIC for bayesian models.

Vehtari, A., Gelman, A., Gabry, J., 2017. Practical bayesian model evaluation using leave-one-out cross-validation and WAIC. Statistics and Computing 27, 1413–1432. https://doi.org/10.1007/s11222-016-9696-4

Vehtari, A., Gelman, A., Simpson, D., Carpenter, B., Bürkner, P.-C., 2021. Rank-normalization, folding, and localization: An improved $\widehat{R}$ for assessing convergence of MCMC. Bayesian Analysis 16. https://doi.org/10.1214/20-BA1221

Wallach, D., Goffinet, B., Bergez, J.-E., Debaeke, P., Leenhardt, D., Aubertot, J.-N., 2001. Parameter estimation for crop models. Agronomy Journal 93, 757–766. https://doi.org/10.2134/agronj2001.934757x

Wang, E., Engel, T., 1998. Simulation of phenological development of wheat crops. Agricultural Systems 58, 1–24. https://doi.org/10.1016/S0308-521X(98)00028-6

Yao, Y., Vehtari, A., Simpson, D., Gelman, A., 2017. Using stacking to average bayesian predictive distributions. Bayesian Analysis. https://doi.org/10.1214/17-BA1091

9 Supporting information

$$
\boldsymbol{\Sigma}_b = \begin{bmatrix}
\sigma^2_{b_0^{D_{R0\text{-}R1}}} & \sigma_{b_0^{D_{R0\text{-}R1}} b_0^{D_{R1\text{-}R3}}} & \sigma_{b_0^{D_{R0\text{-}R1}} b_0^{D_{R3\text{-}R5}}} & \sigma_{b_0^{D_{R0\text{-}R1}} b_0^{D_{R5\text{-}R6}}} & \sigma_{b_0^{D_{R0\text{-}R1}} b_0^{D_{R6\text{-}R7}}} & \sigma_{b_0^{D_{R0\text{-}R1}} b_0^{D_{R7\text{-}R8}}} & \sigma_{b_0^{D_{R0\text{-}R1}} b_0^{T_{\mathrm{hSO\text{-}R1}}}} & \sigma_{b_0^{D_{R0\text{-}R1}} b_0^{T_{\mathrm{hR1\text{-}R5}}}} & \sigma_{b_0^{D_{R0\text{-}R1}} b_0^{T_{\mathrm{hR5\text{-}R7}}}} & \sigma_{b_0^{D_{R0\text{-}R1}} b_0^{P_o}} & \sigma_{b_0^{D_{R0\text{-}R1}} b_0^{P_s}} & \sigma_{b_0^{D_{R0\text{-}R1}} b_0^{\Delta P_o}} \\
\sigma_{b_0^{D_{R1\text{-}R3}} b_0^{D_{R0\text{-}R1}}} & \sigma^2_{b_0^{D_{R1\text{-}R3}}} & \sigma_{b_0^{D_{R1\text{-}R3}} b_0^{D_{R3\text{-}R5}}} & \sigma_{b_0^{D_{R1\text{-}R3}} b_0^{D_{R5\text{-}R6}}} & \sigma_{b_0^{D_{R1\text{-}R3}} b_0^{D_{R6\text{-}R7}}} & \sigma_{b_0^{D_{R1\text{-}R3}} b_0^{D_{R7\text{-}R8}}} & \sigma_{b_0^{D_{R1\text{-}R3}} b_0^{T_{\mathrm{hSO\text{-}R1}}}} & \sigma_{b_0^{D_{R1\text{-}R3}} b_0^{T_{\mathrm{hR1\text{-}R5}}}} & \sigma_{b_0^{D_{R1\text{-}R3}} b_0^{T_{\mathrm{hR5\text{-}R7}}}} & \sigma_{b_0^{D_{R1\text{-}R3}} b_0^{P_o}} & \sigma_{b_0^{D_{R1\text{-}R3}} b_0^{P_s}} & \sigma_{b_0^{D_{R1\text{-}R3}} b_0^{\Delta P_o}} \\
\sigma_{b_0^{D_{R3\text{-}R5}} b_0^{D_{R0\text{-}R1}}} & \sigma_{b_0^{D_{R3\text{-}R5}} b_0^{D_{R1\text{-}R3}}} & \sigma^2_{b_0^{D_{R3\text{-}R5}}} & \sigma_{b_0^{D_{R3\text{-}R5}} b_0^{D_{R5\text{-}R6}}} & \sigma_{b_0^{D_{R3\text{-}R5}} b_0^{D_{R6\text{-}R7}}} & \sigma_{b_0^{D_{R3\text{-}R5}} b_0^{D_{R7\text{-}R8}}} & \sigma_{b_0^{D_{R3\text{-}R5}} b_0^{T_{\mathrm{hSO\text{-}R1}}}} & \sigma_{b_0^{D_{R3\text{-}R5}} b_0^{T_{\mathrm{hR1\text{-}R5}}}} & \sigma_{b_0^{D_{R3\text{-}R5}} b_0^{T_{\mathrm{hR5\text{-}R7}}}} & \sigma_{b_0^{D_{R3\text{-}R5}} b_0^{P_o}} & \sigma_{b_0^{D_{R3\text{-}R5}} b_0^{P_s}} & \sigma_{b_0^{D_{R3\text{-}R5}} b_0^{\Delta P_o}} \\
\sigma_{b_0^{D_{R5\text{-}R6}} b_0^{D_{R0\text{-}R1}}} & \sigma_{b_0^{D_{R5\text{-}R6}} b_0^{D_{R1\text{-}R3}}} & \sigma_{b_0^{D_{R5\text{-}R6}} b_0^{D_{R3\text{-}R5}}} & \sigma^2_{b_0^{D_{R5\text{-}R6}}} & \sigma_{b_0^{D_{R5\text{-}R6}} b_0^{D_{R6\text{-}R7}}} & \sigma_{b_0^{D_{R5\text{-}R6}} b_0^{D_{R7\text{-}R8}}} & \sigma_{b_0^{D_{R5\text{-}R6}} b_0^{T_{\mathrm{hSO\text{-}R1}}}} & \sigma_{b_0^{D_{R5\text{-}R6}} b_0^{T_{\mathrm{hR1\text{-}R5}}}} & \sigma_{b_0^{D_{R5\text{-}R6}} b_0^{T_{\mathrm{hR5\text{-}R7}}}} & \sigma_{b_0^{D_{R5\text{-}R6}} b_0^{P_o}} & \sigma_{b_0^{D_{R5\text{-}R6}} b_0^{P_s}} & \sigma_{b_0^{D_{R5\text{-}R6}} b_0^{\Delta P_o}} \\
\sigma_{b_0^{D_{R6\text{-}R7}} b_0^{D_{R0\text{-}R1}}} & \sigma_{b_0^{D_{R6\text{-}R7}} b_0^{D_{R1\text{-}R3}}} & \sigma_{b_0^{D_{R6\text{-}R7}} b_0^{D_{R3\text{-}R5}}} & \sigma_{b_0^{D_{R6\text{-}R7}} b_0^{D_{R5\text{-}R6}}} & \sigma^2_{b_0^{D_{R6\text{-}R7}}} & \sigma_{b_0^{D_{R6\text{-}R7}} b_0^{D_{R7\text{-}R8}}} & \sigma_{b_0^{D_{R6\text{-}R7}} b_0^{T_{\mathrm{hSO\text{-}R1}}}} & \sigma_{b_0^{D_{R6\text{-}R7}} b_0^{T_{\mathrm{hR1\text{-}R5}}}} & \sigma_{b_0^{D_{R6\text{-}R7}} b_0^{T_{\mathrm{hR5\text{-}R7}}}} & \sigma_{b_0^{D_{R6\text{-}R7}} b_0^{P_o}} & \sigma_{b_0^{D_{R6\text{-}R7}} b_0^{P_s}} & \sigma_{b_0^{D_{R6\text{-}R7}} b_0^{\Delta P_o}} \\
\sigma_{b_0^{D_{R7\text{-}R8}} b_0^{D_{R0\text{-}R1}}} & \sigma_{b_0^{D_{R7\text{-}R8}} b_0^{D_{R1\text{-}R3}}} & \sigma_{b_0^{D_{R7\text{-}R8}} b_0^{D_{R3\text{-}R5}}} & \sigma_{b_0^{D_{R7\text{-}R8}} b_0^{D_{R5\text{-}R6}}} & \sigma_{b_0^{D_{R7\text{-}R8}} b_0^{D_{R6\text{-}R7}}} & \sigma^2_{b_0^{D_{R7\text{-}R8}}} & \sigma_{b_0^{D_{R7\text{-}R8}} b_0^{T_{\mathrm{hSO\text{-}R1}}}} & \sigma_{b_0^{D_{R7\text{-}R8}} b_0^{T_{\mathrm{hR1\text{-}R5}}}} & \sigma_{b_0^{D_{R7\text{-}R8}} b_0^{T_{\mathrm{hR5\text{-}R7}}}} & \sigma_{b_0^{D_{R7\text{-}R8}} b_0^{P_o}} & \sigma_{b_0^{D_{R7\text{-}R8}} b_0^{P_s}} & \sigma_{b_0^{D_{R7\text{-}R8}} b_0^{\Delta P_o}} \\
\sigma_{b_0^{T_{\mathrm{hSO\text{-}R1}}} b_0^{D_{R0\text{-}R1}}} & \sigma_{b_0^{T_{\mathrm{hSO\text{-}R1}}} b_0^{D_{R1\text{-}R3}}} & \sigma_{b_0^{T_{\mathrm{hSO\text{-}R1}}} b_0^{D_{R3\text{-}R5}}} & \sigma_{b_0^{T_{\mathrm{hSO\text{-}R1}}} b_0^{D_{R5\text{-}R6}}} & \sigma_{b_0^{T_{\mathrm{hSO\text{-}R1}}} b_0^{D_{R6\text{-}R7}}} & \sigma_{b_0^{T_{\mathrm{hSO\text{-}R1}}} b_0^{D_{R7\text{-}R8}}} & \sigma^2_{b_0^{T_{\mathrm{hSO\text{-}R1}}}} & \sigma_{b_0^{T_{\mathrm{hSO\text{-}R1}}} b_0^{T_{\mathrm{hR1\text{-}R5}}}} & \sigma_{b_0^{T_{\mathrm{hSO\text{-}R1}}} b_0^{T_{\mathrm{hR5\text{-}R7}}}} & \sigma_{b_0^{T_{\mathrm{hSO\text{-}R1}}} b_0^{P_o}} & \sigma_{b_0^{T_{\mathrm{hSO\text{-}R1}}} b_0^{P_s}} & \sigma_{b_0^{T_{\mathrm{hSO\text{-}R1}}} b_0^{\Delta P_o}} \\
\sigma_{b_0^{T_{\mathrm{hR1\text{-}R5}}} b_0^{D_{R0\text{-}R1}}} & \sigma_{b_0^{T_{\mathrm{hR1\text{-}R5}}} b_0^{D_{R1\text{-}R3}}} & \sigma_{b_0^{T_{\mathrm{hR1\text{-}R5}}} b_0^{D_{R3\text{-}R5}}} & \sigma_{b_0^{T_{\mathrm{hR1\text{-}R5}}} b_0^{D_{R5\text{-}R6}}} & \sigma_{b_0^{T_{\mathrm{hR1\text{-}R5}}} b_0^{D_{R6\text{-}R7}}} & \sigma_{b_0^{T_{\mathrm{hR1\text{-}R5}}} b_0^{D_{R7\text{-}R8}}} & \sigma_{b_0^{T_{\mathrm{hR1\text{-}R5}}} b_0^{T_{\mathrm{hSO\text{-}R1}}}} & \sigma^2_{b_0^{T_{\mathrm{hR1\text{-}R5}}}} & \sigma_{b_0^{T_{\mathrm{hR1\text{-}R5}}} b_0^{T_{\mathrm{hR5\text{-}R7}}}} & \sigma_{b_0^{T_{\mathrm{hR1\text{-}R5}}} b_0^{P_o}} & \sigma_{b_0^{T_{\mathrm{hR1\text{-}R5}}} b_0^{P_s}} & \sigma_{b_0^{T_{\mathrm{hR1\text{-}R5}}} b_0^{\Delta P_o}} \\
\sigma_{b_0^{T_{\mathrm{hR5\text{-}R7}}} b_0^{D_{R0\text{-}R1}}} & \sigma_{b_0^{T_{\mathrm{hR5\text{-}R7}}} b_0^{D_{R1\text{-}R3}}} & \sigma_{b_0^{T_{\mathrm{hR5\text{-}R7}}} b_0^{D_{R3\text{-}R5}}} & \sigma_{b_0^{T_{\mathrm{hR5\text{-}R7}}} b_0^{D_{R5\text{-}R6}}} & \sigma_{b_0^{T_{\mathrm{hR5\text{-}R7}}} b_0^{D_{R6\text{-}R7}}} & \sigma_{b_0^{T_{\mathrm{hR5\text{-}R7}}} b_0^{D_{R7\text{-}R8}}} & \sigma_{b_0^{T_{\mathrm{hR5\text{-}R7}}} b_0^{T_{\mathrm{hSO\text{-}R1}}}} & \sigma_{b_0^{T_{\mathrm{hR5\text{-}R7}}} b_0^{T_{\mathrm{hR1\text{-}R5}}}} & \sigma^2_{b_0^{T_{\mathrm{hR5\text{-}R7}}}} & \sigma_{b_0^{T_{\mathrm{hR5\text{-}R7}}} b_0^{P_o}} & \sigma_{b_0^{T_{\mathrm{hR5\text{-}R7}}} b_0^{P_s}} & \sigma_{b_0^{T_{\mathrm{hR5\text{-}R7}}} b_0^{\Delta P_o}} \\
\sigma_{b_0^{P_o} b_0^{D_{R0\text{-}R1}}} & \sigma_{b_0^{P_o} b_0^{D_{R1\text{-}R3}}} & \sigma_{b_0^{P_o} b_0^{D_{R3\text{-}R5}}} & \sigma_{b_0^{P_o} b_0^{D_{R5\text{-}R6}}} & \sigma_{b_0^{P_o} b_0^{D_{R6\text{-}R7}}} & \sigma_{b_0^{P_o} b_0^{D_{R7\text{-}R8}}} & \sigma_{b_0^{P_o} b_0^{T_{\mathrm{hSO\text{-}R1}}}} & \sigma_{b_0^{P_o} b_0^{T_{\mathrm{hR1\text{-}R5}}}} & \sigma_{b_0^{P_o} b_0^{T_{\mathrm{hR5\text{-}R7}}}} & \sigma^2_{b_0^{P_o}} & \sigma_{b_0^{P_o} b_0^{P_s}} & \sigma_{b_0^{P_o} b_0^{\Delta P_o}} \\
\sigma_{b_0^{P_s} b_0^{D_{R0\text{-}R1}}} & \sigma_{b_0^{P_s} b_0^{D_{R1\text{-}R3}}} & \sigma_{b_0^{P_s} b_0^{D_{R3\text{-}R5}}} & \sigma_{b_0^{P_s} b_0^{D_{R5\text{-}R6}}} & \sigma_{b_0^{P_s} b_0^{D_{R6\text{-}R7}}} & \sigma_{b_0^{P_s} b_0^{D_{R7\text{-}R8}}} & \sigma_{b_0^{P_s} b_0^{T_{\mathrm{hSO\text{-}R1}}}} & \sigma_{b_0^{P_s} b_0^{T_{\mathrm{hR1\text{-}R5}}}} & \sigma_{b_0^{P_s} b_0^{T_{\mathrm{hR5\text{-}R7}}}} & \sigma_{b_0^{P_s} b_0^{P_o}} & \sigma^2_{b_0^{P_s}} & \sigma_{b_0^{P_s} b_0^{\Delta P_o}} \\
\sigma_{b_0^{\Delta P_o} b_0^{D_{R0\text{-}R1}}} & \sigma_{b_0^{\Delta P_o} b_0^{D_{R1\text{-}R3}}} & \sigma_{b_0^{\Delta P_o} b_0^{D_{R3\text{-}R5}}} & \sigma_{b_0^{\Delta P_o} b_0^{D_{R5\text{-}R6}}} & \sigma_{b_0^{\Delta P_o} b_0^{D_{R6\text{-}R7}}} & \sigma_{b_0^{\Delta P_o} b_0^{D_{R7\text{-}R8}}} & \sigma_{b_0^{\Delta P_o} b_0^{T_{\mathrm{hSO\text{-}R1}}}} & \sigma_{b_0^{\Delta P_o} b_0^{T_{\mathrm{hR1\text{-}R5}}}} & \sigma_{b_0^{\Delta P_o} b_0^{T_{\mathrm{hR5\text{-}R7}}}} & \sigma_{b_0^{\Delta P_o} b_0^{P_o}} & \sigma_{b_0^{\Delta P_o} b_0^{P_s}} & \sigma^2_{b_0^{\Delta P_o}}
\end{bmatrix} \tag{36}
$$

$$
\boldsymbol{\Sigma}_\epsilon = \begin{bmatrix}
\sigma^2_{\epsilon^{D_{R0\text{-}R1}}} & \sigma_{\epsilon^{D_{R0\text{-}R1}} \epsilon^{D_{R1\text{-}R3}}} & \sigma_{\epsilon^{D_{R0\text{-}R1}} \epsilon^{D_{R3\text{-}R5}}} & \sigma_{\epsilon^{D_{R0\text{-}R1}} \epsilon^{D_{R5\text{-}R6}}} & \sigma_{\epsilon^{D_{R0\text{-}R1}} \epsilon^{D_{R6\text{-}R7}}} & \sigma_{\epsilon^{D_{R0\text{-}R1}} \epsilon^{D_{R7\text{-}R8}}} & \sigma_{\epsilon^{D_{R0\text{-}R1}} \epsilon^{T_{\mathrm{hSO\text{-}R1}}}} & \sigma_{\epsilon^{D_{R0\text{-}R1}} \epsilon^{T_{\mathrm{hR1\text{-}R5}}}} & \sigma_{\epsilon^{D_{R0\text{-}R1}} \epsilon^{T_{\mathrm{hR5\text{-}R7}}}} & \sigma_{\epsilon^{D_{R0\text{-}R1}} \epsilon^{P_o}} & \sigma_{\epsilon^{D_{R0\text{-}R1}} \epsilon^{P_s}} & \sigma_{\epsilon^{D_{R0\text{-}R1}} \epsilon^{\Delta P_o}} \\
\sigma_{\epsilon^{D_{R1\text{-}R3}} \epsilon^{D_{R0\text{-}R1}}} & \sigma^2_{\epsilon^{D_{R1\text{-}R3}}} & \sigma_{\epsilon^{D_{R1\text{-}R3}} \epsilon^{D_{R3\text{-}R5}}} & \sigma_{\epsilon^{D_{R1\text{-}R3}} \epsilon^{D_{R5\text{-}R6}}} & \sigma_{\epsilon^{D_{R1\text{-}R3}} \epsilon^{D_{R6\text{-}R7}}} & \sigma_{\epsilon^{D_{R1\text{-}R3}} \epsilon^{D_{R7\text{-}R8}}} & \sigma_{\epsilon^{D_{R1\text{-}R3}} \epsilon^{T_{\mathrm{hSO\text{-}R1}}}} & \sigma_{\epsilon^{D_{R1\text{-}R3}} \epsilon^{T_{\mathrm{hR1\text{-}R5}}}} & \sigma_{\epsilon^{D_{R1\text{-}R3}} \epsilon^{T_{\mathrm{hR5\text{-}R7}}}} & \sigma_{\epsilon^{D_{R1\text{-}R3}} \epsilon^{P_o}} & \sigma_{\epsilon^{D_{R1\text{-}R3}} \epsilon^{P_s}} & \sigma_{\epsilon^{D_{R1\text{-}R3}} \epsilon^{\Delta P_o}} \\
\sigma_{\epsilon^{D_{R3\text{-}R5}} \epsilon^{D_{R0\text{-}R1}}} & \sigma_{\epsilon^{D_{R3\text{-}R5}} \epsilon^{D_{R1\text{-}R3}}} & \sigma^2_{\epsilon^{D_{R3\text{-}R5}}} & \sigma_{\epsilon^{D_{R3\text{-}R5}} \epsilon^{D_{R5\text{-}R6}}} & \sigma_{\epsilon^{D_{R3\text{-}R5}} \epsilon^{D_{R6\text{-}R7}}} & \sigma_{\epsilon^{D_{R3\text{-}R5}} \epsilon^{D_{R7\text{-}R8}}} & \sigma_{\epsilon^{D_{R3\text{-}R5}} \epsilon^{T_{\mathrm{hSO\text{-}R1}}}} & \sigma_{\epsilon^{D_{R3\text{-}R5}} \epsilon^{T_{\mathrm{hR1\text{-}R5}}}} & \sigma_{\epsilon^{D_{R3\text{-}R5}} \epsilon^{T_{\mathrm{hR5\text{-}R7}}}} & \sigma_{\epsilon^{D_{R3\text{-}R5}} \epsilon^{P_o}} & \sigma_{\epsilon^{D_{R3\text{-}R5}} \epsilon^{P_s}} & \sigma_{\epsilon^{D_{R3\text{-}R5}} \epsilon^{\Delta P_o}} \\
\sigma_{\epsilon^{D_{R5\text{-}R6}} \epsilon^{D_{R0\text{-}R1}}} & \sigma_{\epsilon^{D_{R5\text{-}R6}} \epsilon^{D_{R1\text{-}R3}}} & \sigma_{\epsilon^{D_{R5\text{-}R6}} \epsilon^{D_{R3\text{-}R5}}} & \sigma^2_{\epsilon^{D_{R5\text{-}R6}}} & \sigma_{\epsilon^{D_{R5\text{-}R6}} \epsilon^{D_{R6\text{-}R7}}} & \sigma_{\epsilon^{D_{R5\text{-}R6}} \epsilon^{D_{R7\text{-}R8}}} & \sigma_{\epsilon^{D_{R5\text{-}R6}} \epsilon^{T_{\mathrm{hSO\text{-}R1}}}} & \sigma_{\epsilon^{D_{R5\text{-}R6}} \epsilon^{T_{\mathrm{hR1\text{-}R5}}}} & \sigma_{\epsilon^{D_{R5\text{-}R6}} \epsilon^{T_{\mathrm{hR5\text{-}R7}}}} & \sigma_{\epsilon^{D_{R5\text{-}R6}} \epsilon^{P_o}} & \sigma_{\epsilon^{D_{R5\text{-}R6}} \epsilon^{P_s}} & \sigma_{\epsilon^{D_{R5\text{-}R6}} \epsilon^{\Delta P_o}} \\
\sigma_{\epsilon^{D_{R6\text{-}R7}} \epsilon^{D_{R0\text{-}R1}}} & \sigma_{\epsilon^{D_{R6\text{-}R7}} \epsilon^{D_{R1\text{-}R3}}} & \sigma_{\epsilon^{D_{R6\text{-}R7}} \epsilon^{D_{R3\text{-}R5}}} & \sigma_{\epsilon^{D_{R6\text{-}R7}} \epsilon^{D_{R5\text{-}R6}}} & \sigma^2_{\epsilon^{D_{R6\text{-}R7}}} & \sigma_{\epsilon^{D_{R6\text{-}R7}} \epsilon^{D_{R7\text{-}R8}}} & \sigma_{\epsilon^{D_{R6\text{-}R7}} \epsilon^{T_{\mathrm{hSO\text{-}R1}}}} & \sigma_{\epsilon^{D_{R6\text{-}R7}} \epsilon^{T_{\mathrm{hR1\text{-}R5}}}} & \sigma_{\epsilon^{D_{R6\text{-}R7}} \epsilon^{T_{\mathrm{hR5\text{-}R7}}}} & \sigma_{\epsilon^{D_{R6\text{-}R7}} \epsilon^{P_o}} & \sigma_{\epsilon^{D_{R6\text{-}R7}} \epsilon^{P_s}} & \sigma_{\epsilon^{D_{R6\text{-}R7}} \epsilon^{\Delta P_o}} \\
\sigma_{\epsilon^{D_{R7\text{-}R8}} \epsilon^{D_{R0\text{-}R1}}} & \sigma_{\epsilon^{D_{R7\text{-}R8}} \epsilon^{D_{R1\text{-}R3}}} & \sigma_{\epsilon^{D_{R7\text{-}R8}} \epsilon^{D_{R3\text{-}R5}}} & \sigma_{\epsilon^{D_{R7\text{-}R8}} \epsilon^{D_{R5\text{-}R6}}} & \sigma_{\epsilon^{D_{R7\text{-}R8}} \epsilon^{D_{R6\text{-}R7}}} & \sigma^2_{\epsilon^{D_{R7\text{-}R8}}} & \sigma_{\epsilon^{D_{R7\text{-}R8}} \epsilon^{T_{\mathrm{hSO\text{-}R1}}}} & \sigma_{\epsilon^{D_{R7\text{-}R8}} \epsilon^{T_{\mathrm{hR1\text{-}R5}}}} & \sigma_{\epsilon^{D_{R7\text{-}R8}} \epsilon^{T_{\mathrm{hR5\text{-}R7}}}} & \sigma_{\epsilon^{D_{R7\text{-}R8}} \epsilon^{P_o}} & \sigma_{\epsilon^{D_{R7\text{-}R8}} \epsilon^{P_s}} & \sigma_{\epsilon^{D_{R7\text{-}R8}} \epsilon^{\Delta P_o}} \\
\sigma_{\epsilon^{T_{\mathrm{hSO\text{-}R1}}} \epsilon^{D_{R0\text{-}R1}}} & \sigma_{\epsilon^{T_{\mathrm{hSO\text{-}R1}}} \epsilon^{D_{R1\text{-}R3}}} & \sigma_{\epsilon^{T_{\mathrm{hSO\text{-}R1}}} \epsilon^{D_{R3\text{-}R5}}} & \sigma_{\epsilon^{T_{\mathrm{hSO\text{-}R1}}} \epsilon^{D_{R5\text{-}R6}}} & \sigma_{\epsilon^{T_{\mathrm{hSO\text{-}R1}}} \epsilon^{D_{R6\text{-}R7}}} & \sigma_{\epsilon^{T_{\mathrm{hSO\text{-}R1}}} \epsilon^{D_{R7\text{-}R8}}} & \sigma^2_{\epsilon^{T_{\mathrm{hSO\text{-}R1}}}} & \sigma_{\epsilon^{T_{\mathrm{hSO\text{-}R1}}} \epsilon^{T_{\mathrm{hR1\text{-}R5}}}} & \sigma_{\epsilon^{T_{\mathrm{hSO\text{-}R1}}} \epsilon^{T_{\mathrm{hR5\text{-}R7}}}} & \sigma_{\epsilon^{T_{\mathrm{hSO\text{-}R1}}} \epsilon^{P_o}} & \sigma_{\epsilon^{T_{\mathrm{hSO\text{-}R1}}} \epsilon^{P_s}} & \sigma_{\epsilon^{T_{\mathrm{hSO\text{-}R1}}} \epsilon^{\Delta P_o}} \\
\sigma_{\epsilon^{T_{\mathrm{hR1\text{-}R5}}} \epsilon^{D_{R0\text{-}R1}}} & \sigma_{\epsilon^{T_{\mathrm{hR1\text{-}R5}}} \epsilon^{D_{R1\text{-}R3}}} & \sigma_{\epsilon^{T_{\mathrm{hR1\text{-}R5}}} \epsilon^{D_{R3\text{-}R5}}} & \sigma_{\epsilon^{T_{\mathrm{hR1\text{-}R5}}} \epsilon^{D_{R5\text{-}R6}}} & \sigma_{\epsilon^{T_{\mathrm{hR1\text{-}R5}}} \epsilon^{D_{R6\text{-}R7}}} & \sigma_{\epsilon^{T_{\mathrm{hR1\text{-}R5}}} \epsilon^{D_{R7\text{-}R8}}} & \sigma_{\epsilon^{T_{\mathrm{hR1\text{-}R5}}} \epsilon^{T_{\mathrm{hSO\text{-}R1}}}} & \sigma^2_{\epsilon^{T_{\mathrm{hR1\text{-}R5}}}} & \sigma_{\epsilon^{T_{\mathrm{hR1\text{-}R5}}} \epsilon^{T_{\mathrm{hR5\text{-}R7}}}} & \sigma_{\epsilon^{T_{\mathrm{hR1\text{-}R5}}} \epsilon^{P_o}} & \sigma_{\epsilon^{T_{\mathrm{hR1\text{-}R5}}} \epsilon^{P_s}} & \sigma_{\epsilon^{T_{\mathrm{hR1\text{-}R5}}} \epsilon^{\Delta P_o}} \\
\sigma_{\epsilon^{T_{\mathrm{hR5\text{-}R7}}} \epsilon^{D_{R0\text{-}R1}}} & \sigma_{\epsilon^{T_{\mathrm{hR5\text{-}R7}}} \epsilon^{D_{R1\text{-}R3}}} & \sigma_{\epsilon^{T_{\mathrm{hR5\text{-}R7}}} \epsilon^{D_{R3\text{-}R5}}} & \sigma_{\epsilon^{T_{\mathrm{hR5\text{-}R7}}} \epsilon^{D_{R5\text{-}R6}}} & \sigma_{\epsilon^{T_{\mathrm{hR5\text{-}R7}}} \epsilon^{D_{R6\text{-}R7}}} & \sigma_{\epsilon^{T_{\mathrm{hR5\text{-}R7}}} \epsilon^{D_{R7\text{-}R8}}} & \sigma_{\epsilon^{T_{\mathrm{hR5\text{-}R7}}} \epsilon^{T_{\mathrm{hSO\text{-}R1}}}} & \sigma_{\epsilon^{T_{\mathrm{hR5\text{-}R7}}} \epsilon^{T_{\mathrm{hR1\text{-}R5}}}} & \sigma^2_{\epsilon^{T_{\mathrm{hR5\text{-}R7}}}} & \sigma_{\epsilon^{T_{\mathrm{hR5\text{-}R7}}} \epsilon^{P_o}} & \sigma_{\epsilon^{T_{\mathrm{hR5\text{-}R7}}} \epsilon^{P_s}} & \sigma_{\epsilon^{T_{\mathrm{hR5\text{-}R7}}} \epsilon^{\Delta P_o}} \\
\sigma_{\epsilon^{P_o} \epsilon^{D_{R0\text{-}R1}}} & \sigma_{\epsilon^{P_o} \epsilon^{D_{R1\text{-}R3}}} & \sigma_{\epsilon^{P_o} \epsilon^{D_{R3\text{-}R5}}} & \sigma_{\epsilon^{P_o} \epsilon^{D_{R5\text{-}R6}}} & \sigma_{\epsilon^{P_o} \epsilon^{D_{R6\text{-}R7}}} & \sigma_{\epsilon^{P_o} \epsilon^{D_{R7\text{-}R8}}} & \sigma_{\epsilon^{P_o} \epsilon^{T_{\mathrm{hSO\text{-}R1}}}} & \sigma_{\epsilon^{P_o} \epsilon^{T_{\mathrm{hR1\text{-}R5}}}} & \sigma_{\epsilon^{P_o} \epsilon^{T_{\mathrm{hR5\text{-}R7}}}} & \sigma^2_{\epsilon^{P_o}} & \sigma_{\epsilon^{P_o} \epsilon^{P_s}} & \sigma_{\epsilon^{P_o} \epsilon^{\Delta P_o}} \\
\sigma_{\epsilon^{P_s} \epsilon^{D_{R0\text{-}R1}}} & \sigma_{\epsilon^{P_s} \epsilon^{D_{R1\text{-}R3}}} & \sigma_{\epsilon^{P_s} \epsilon^{D_{R3\text{-}R5}}} & \sigma_{\epsilon^{P_s} \epsilon^{D_{R5\text{-}R6}}} & \sigma_{\epsilon^{P_s} \epsilon^{D_{R6\text{-}R7}}} & \sigma_{\epsilon^{P_s} \epsilon^{D_{R7\text{-}R8}}} & \sigma_{\epsilon^{P_s} \epsilon^{T_{\mathrm{hSO\text{-}R1}}}} & \sigma_{\epsilon^{P_s} \epsilon^{T_{\mathrm{hR1\text{-}R5}}}} & \sigma_{\epsilon^{P_s} \epsilon^{T_{\mathrm{hR5\text{-}R7}}}} & \sigma_{\epsilon^{P_s} \epsilon^{P_o}} & \sigma^2_{\epsilon^{P_s}} & \sigma_{\epsilon^{P_s} \epsilon^{\Delta P_o}} \\
\sigma_{\epsilon^{\Delta P_o} \epsilon^{D_{R0\text{-}R1}}} & \sigma_{\epsilon^{\Delta P_o} \epsilon^{D_{R1\text{-}R3}}} & \sigma_{\epsilon^{\Delta P_o} \epsilon^{D_{R3\text{-}R5}}} & \sigma_{\epsilon^{\Delta P_o} \epsilon^{D_{R5\text{-}R6}}} & \sigma_{\epsilon^{\Delta P_o} \epsilon^{D_{R6\text{-}R7}}} & \sigma_{\epsilon^{\Delta P_o} \epsilon^{D_{R7\text{-}R8}}} & \sigma_{\epsilon^{\Delta P_o} \epsilon^{T_{\mathrm{hSO\text{-}R1}}}} & \sigma_{\epsilon^{\Delta P_o} \epsilon^{T_{\mathrm{hR1\text{-}R5}}}} & \sigma_{\epsilon^{\Delta P_o} \epsilon^{T_{\mathrm{hR5\text{-}R7}}}} & \sigma_{\epsilon^{\Delta P_o} \epsilon^{P_o}} & \sigma_{\epsilon^{\Delta P_o} \epsilon^{P_s}} & \sigma^2_{\epsilon^{\Delta P_o}}
\end{bmatrix} \tag{37}
$$